Eur. Phys. J. C (2026) 86:431
https://doi.org/10.1140/epjc/s10052-026-15673-5

THE EUROPEAN PHYSICAL JOURNAL C

Regular Article - Theoretical Physics

Light neutral Higgs-boson production at e^+e^- colliders in the complex MSSM and NMSSM: a full one-loop analysis

S. Heinemeyer[1,a], **S. Passehr**[2,b], **C. Schappacher**[3,c]

[1] Instituto de Física Teórica (UAM/CSIC), Universidad Autónoma de Madrid, Cantoblanco, 28049 Madrid, Spain
[2] Institute for Theoretical Particle Physics and Cosmology, RWTH Aachen University, Sommerfeldstraße 16, 52074 Aachen, Germany
[3] Institut für Theoretische Physik, Karlsruhe Institute of Technology, 76128 Karlsruhe, Germany

Received: 21 July 2025 / Accepted: 7 April 2026

Abstract For future precision analyses of the Higgs boson at $\approx$ 125 GeV, h_{125}, a precise knowledge of its production and decay properties is mandatory. While in the Standard Model (SM) these calculations are quite advanced, in many models beyond the SM (BSM) a precise calculation is missing so far. We present the calculation of the Higgs-strahlung cross-sections at e^+e^- colliders for the light neutral Higgs boson production in the next-to-minimal supersymmetric SM (NMSSM) with complex parameters (cNMSSM). The evaluation is based on a full one-loop calculation of the production mechanism $e^+e^- \to h_1 Z$, including soft, hard, and collinear photon radiation. The dependence of the Higgs boson production cross-sections on the relevant cNMSSM parameters is analyzed numerically. In certain scenarios we find sizable corrections to the Higgs-strahlung cross-section. Normally, they reach about 10% of the tree-level results, but can also exceed 20%. Finally, the calculation is compared to the corresponding one in the Minimal Supersymmetric SM (MSSM). The knowledge of the full one-loop contributions to the Higgs-boson production is particularly important for a sound theoretical interpretation of measurements at future e^+e^- colliders such as the ILC, CLIC, LCF, FCC-ee, or CEPC. It is planned to implement the evaluation of the Higgs boson production cross-sections into an add-on package to the code `FeynHiggs`.

1 Introduction

The discovery of a new particle with a mass of about 125 GeV in the Higgs searches at the Large Hadron Collider (LHC) about 12 years ago by ATLAS [1] and CMS [2], marks the culmination of an effort that has been ongoing for more than half a century and opens a new era of particle physics. Within the experimental and theoretical uncertainties the measured properties of the newly discovered particle are, so far, in agreement with a Higgs boson as predicted in the Standard Model (SM) [3,4]. However, the experimental results for the state at $\approx$ 125 GeV, whose couplings are known up to now to an experimental precision of roughly $\sim$ 10–20%, leave ample room for interpretations in models beyond the SM (BSM).

The identification of the underlying physics of the discovered new particle and the exploration of the mechanism of electroweak symmetry breaking will clearly be a top priority in the future program of particle physics. The most frequently studied theories incorporating a Higgs particle with the measured properties are the SM, and extensions of the SM by another Higgs doublets and possibly an additional singlet. The latter two scenarios can be further enriched by incorporating supersymmetry (SUSY) into the model, yielding the Minimal Supersymmetric SM (MSSM) [5–10] and the Next-to MSSM (NMSSM) [11,12], respectively. The extension of the MSSM by a gauge-singlet superfield was originally motivated by the 'μ problem' [13,14].[1] Contrary to the case of the SM, as mentioned above, two complex Higgs doublets are required in the MSSM, which are extended further by a complex Higgs singlet in the NMSSM. This results in five

Former address: S. Passehr, C. Schappacher.

[a] e-mail: Sven.Heinemeyer@cern.ch (corresponding author)
[b] e-mail: sebastian.passehr@web.de
[c] e-mail: schappacher@kabelbw.de

[1] It should be noted that the NMSSM itself possibly suffers from a domain wall problem due to the Z_3 breaking. However, many suggestions to avoid this problem have been proposed [15–22].

Published online: 29 April 2026

or seven physical Higgs bosons in the MSSM or NMSSM instead of the single physical Higgs boson in the SM. At lowest order in the MSSM these are the light and heavy $\mathcal{CP}$-even Higgs bosons, h and H, the $\mathcal{CP}$-odd Higgs boson, A, and two charged Higgs bosons, $H^\pm$. Considering only real parameters, the NMSSM extends the $\mathcal{CP}$-even and $\mathcal{CP}$-odd sectors by one Higgs boson each. In the case of complex parameters (and taking into account higher-order corrections for the MSSM), all neutral Higgs bosons can mix, resulting in h_i $(i = 1, 2, 3)$ in the cMSSM [23–27], or in h_i $(i = 1, 2, 3, 4, 5)$ in the cNMSSM [28]. In this work we will consider in general the cMSSM and the cNMSSM.

The Higgs sector of the cMSSM is described at the tree level by two parameters: the mass of the charged Higgs bosons, $M_{H^\pm}$, and the ratio of the two vacuum-expectation values (VEVs), $\tan\beta \equiv t_\beta = v_2/v_1$. In addition to the two cMSSM-like parameters, the singlet Higgs sector of the cNMSSM introduces four additional independent parameters in the extended Higgs potential. Following the common nomenclature, we choose: λ, κ, A_κ and the VEV of the singlet, v_s. In the cNMSSM, the mu-Parameter of the cMSSM is generated dynamically as $\mu_{\text{eff}} := \lambda\, v_s$. In the scenarios investigated in this paper, we identify the lightest Higgs boson, h_1 with the particle discovered at the LHC at $\approx$ 125 GeV [1,2], h_{125} (see [29] for an original analysis).[2] Here it should be noted that in SUSY models the mass of the Higgs bosons other than the charged one are not free parameters, but can be calculated in terms of the other model parameters, see [30] for a review. This sets important constraints on the SUSY parameter space.

Several possible future e^+e^- colliders are currently under consideration. Circular designs, the FCC-ee [31,32] and the CEPC [33–35], are proposed to start with a center-of-mass energy of $\sqrt{s} = 250$ GeV (going up to $\sim$ 350–365 GeV in the final stage). Linear designs, the ILC [36,37], LCF [38,39] and CLIC [37,40], are proposed to start with $\sqrt{s} =$ 250 GeV and 380 GeV, respectively (going up to 1000 GeV and 3000 GeV in the final stage, respectively). At a future e^+e^- collider several production modes for the neutral Higgs bosons in the cNMSSM are possible, depending on the available center-of-mass energy,

$$e^+e^- \to h_i Z,\ h_i\gamma,\ h_i h_j,\ h_i \nu\bar{\nu},\ h_i e^+e^-,\ h_i t\bar{t},\\ h_i b\bar{b},\ \ldots\ (i, j = 1, 2, 3, 4, 5), \tag{1}$$

where we identify $h_1 \equiv h_{125}$. Taking into account the starting energy of the various possible future e^+e^- colliders, only the production process

$$e^+e^- \to h_{125} Z \tag{2}$$

is accessible with a high rate.[3] at all proposed future experiments. It will serve to measure the couplings of the h_{125} with very high accuracy, see [44] for a review. Roughly speaking, couplings to heavier fermions will be determined at about the per cent level, whereas the couplings to massive gauge bosons can reach the per mille level. Such a precise determination of the h_{125} couplings requires a prediction of its production and decay modes at least at the same level of accuracy. In the following, we will concentrate on the corresponding calculations in the cMSSM and cNMSSM.

In order to yield a sufficient accuracy, one-loop corrections to the various Higgs boson production and decay modes have to be considered. Full one-loop calculations in the cMSSM for various h_{125} decays into SM fermions, but also into their scalar superpartners as well as charginos and neutralinos (which are by now experimentally excluded, except for the decay into a pair of the lightest neutralinos), have been presented over the last years [45–47]. For the decay into SM fermions, see also Refs. [48–54]. Decays into SM gauge bosons (see also [55]) can be evaluated to a very high precision using the full SM one-loop result [56–58] combined with the appropriate effective couplings [59]. The full one-loop corrections in the cMSSM listed here together with resummed SUSY corrections have been implemented into the code `FeynHiggs`[59–67]. Corrections at and beyond the one-loop level in the MSSM with real parameters (rMSSM) are implemented into the code `HDECAY`[68–70]. Both codes were combined by the LHC Higgs Cross Section Working Group to obtain the most precise evaluation for rMSSM Higgs boson decays [71]. Corresponding calculations in the cNMSSM can be found in Refs. [72–79]. These results have not yet been implemented into a public computer code.

In the above-cited papers it was concluded that the required level of precision in the h_{125} decays is not yet reached, but can be done with known computational techniques. On the other hand, the corresponding precision level of the h_{125} production modes is less advanced. Taking into account the starting energies of the various future e^+e^- collider proposals, from now on we focus on the process in Eq. 2. A full one-loop calculation for the process in Eq. 2 in the cMSSM was presented in [41] (see also [80]). However, these results have not yet been included in a public computer code. No corresponding calculation in the cNMSSM has been published so far. In this work we present a consistent calculation of the process in Eq. 2 in the cMSSM and cNMSSM at the full one-loop level. The "MSSM part" of the NMSSM calculation is performed exactly as in the MSSM. Consequently, differences in the

[2] The results of our paper are equally valid for any (N)MSSM Higgs boson that is identified with the h_{125}.

[3] Also the process $e^+e^- \to h_{125}\gamma$ is kinematically accessible, but has a substantially lower rate [41–43].

predictions of the Higgs boson production cross section can directly be attributed to the differences of the two models.

The evaluation of the channel (2) is based on a full one-loop calculation, i.e. including electroweak (EW) corrections, as well as soft, hard, and collinear photon radiation. The Higgs boson masses are evaluated at the two-loop level (using `NMSSMCALC` (version 5.0) [81–85]). The variety of existing results for the MSSM cross-section calculations have been summarized in [41]. On the other hand, in the NMSSM very few calculations have been performed in the past. In [86] higher-order corrections to the NMSSM Higgs sector were evaluated in the effective-potential approach at the one-loop level, taking into account contributions from 3rd generation quarks and squarks. The corresponding mixing was introduced into the effective ZZh_1 coupling. In [87] the production cross-section for a light singlet-dominated Higgs was evaluated at the tree level. To our knowledge, no full one-loop calculation in the cNMSSM has ever been attempted. Comments about a numerical comparison with the literature will be given in Sect. 3.5.

In this paper we present for the first time a full and consistent one-loop calculation for the production of (light, i.e. corresponding to h_{125}) neutral Higgs bosons in the cNMSSM at e^+e^- colliders in association with a Z boson. We take into account soft, hard and collinear photon emission and the $Z^{\rm mix}$ factor contributions. In this way we go substantially beyond the existing calculations (see above). In Sect. 2 we very briefly review the renormalization of the relevant sectors of the cNMSSM. Details with regards to the calculation can be found in Sect. 3, and we also comment on comparisons with the literature in Sect. 3.5. The numerical results for the channel (2) are presented in Sect. 4. The conclusions can be found in Sect. 5. There are plans to implement the evaluation of the production cross-sections into the Fortran code `FeynHiggs`[59–67].

Prolegomena

We use the following short-hands in this paper:

- $s_{\rm w} \equiv \sin\theta_{\rm w}$, $c_{\rm w} \equiv \cos\theta_{\rm w}$.
- $s_\beta \equiv \sin\beta$, $c_\beta \equiv \cos\beta$, $t_\beta \equiv \tan\beta$, $s_{\beta-\alpha} \equiv \sin(\beta-\alpha)$.

They will be further explained in the text below.

2 The complex (N)MSSM

The cross section Eq. 2 is calculated at the one-loop level (including soft, hard and collinear photon radiation), see the next section. This requires the simultaneous renormalization of the Higgs- and gauge-boson sectors as well as the electron–positron sector of the c(N)MSSM. We give a few relevant details as regards these sectors and their renormalization. More information can be found in Refs. [28,46,47,88–97].

The renormalization of the Higgs and gauge-boson sectors of the cMSSM follows strictly [88] and references therein (see especially [59]). This defines in particular the counterterm δt_β as well as the counterterms for the Z boson mass, δM_Z^2, and for the sine of the weak mixing angle, $\delta s_{\rm w}$ (with $s_{\rm w} = \sqrt{1-c_{\rm w}^2} = \sqrt{1 - M_W^2/M_Z^2}$, where M_W and M_Z denote the W and Z boson masses, respectively).

The renormalization of the fermion sector is described in detail in [88] and references therein. We use the on-shell (OS) renormalization for all three generations of leptons.

Aside from δM_Z^2 and $\delta s_{\rm w}$, and different from the cMSSM, also the electric charge e appears as independent parameter in the tree-level Higgs potential of the cNMSSM and needs to be renormalized at the one-loop order. We choose to fix it via

$$e \to e\,(1+\delta Z_e)\,, \tag{3}$$

$$\delta Z_e = \frac{1}{2}\left(\frac{s_{\rm w}}{c_{\rm w}}\delta Z_{Z\gamma} - \delta Z_{\gamma\gamma}\right)\,, \tag{4}$$

$$\delta Z_{\gamma\gamma} = -\,\widetilde{\rm Re}\,\frac{\partial}{\partial q^2}\,\Sigma_\gamma^T(q^2)\Big|_{q^2=0}\,, \tag{5}$$

$$\delta Z_{Z\gamma} = \frac{2}{M_Z^2}\,\widetilde{\rm Re}\,\Sigma_{\gamma Z}^T(0), \tag{6}$$

where Σ_γ^T and $\Sigma_{\gamma Z}^T$ denote the transverse part of the photon and photon-Z self-energies, respectively. $\widetilde{\rm Re}$ takes the real part of loop integrals only and leaves complex couplings unaffected, see [88].

In extension to the MSSM, in the NMSSM an additional VEV, v_S, is introduced via the Higgs singlet. The corresponding additional minimization conditions following from the singlet tadpoles are utilized to fix the phases of δA_κ and δA_λ (and as usual the bilinear singlet mass parameter, M_S^2, see, e.g. Eq. (2.5) in [12]). The absolute value of δA_λ is determined by the condition for on-shell charged Higgs bosons. The other cNMSSM-specific input parameters are taken to be $\overline{\rm DR}$ parameters, see e.g. [28].

We denote the complex input parameters as:

$$z = |z|\,e^{i\,\varphi_z} \quad \text{with} \quad z = \lambda, \kappa, \mu_{\rm eff}, A_\kappa, A_t\,. \tag{7}$$

The $\overline{\rm DR}$ renormalized parameters λ, κ, A_κ, t_β, and $\mu_{\rm eff}$ run from the input scale, which we take as m_t, to the process scale $Q = m_{h_1} + M_Z$ as follows,

$$\lambda(Q) = \lambda(m_t) + \beta_\lambda\,\ln(Q^2/m_t^2)\,, \tag{8}$$

$$\kappa(Q) = \kappa(m_t) + \beta_\kappa\,\ln(Q^2/m_t^2)\,, \tag{9}$$

$$A_\kappa(Q) = A_\kappa(m_t) + \beta_{A_\kappa}\,\ln(Q^2/m_t^2)\,, \tag{10}$$

$$t_\beta(Q) = t_\beta(m_t) + \beta_{t_\beta}\,\ln(Q^2/m_t^2)\,, \tag{11}$$

$$\mu_{\rm eff}(Q) = \mu_{\rm eff}(m_t) + \beta_{\mu_{\rm eff}} \ln(Q^2/m_t^2)\,, \tag{12}$$

with

$$\beta_\lambda = -\frac{\lambda}{32\pi^2 s_{\rm w}^2 c_{\rm w}^2}\Big[\alpha\pi\,(12 c_{\rm w}^2 + 4 s_{\rm w}^2) - s_{\rm w}^2 c_{\rm w}^2\,(4|\lambda|^2 + 2|\kappa|^2) + Y_\lambda\Big]\,, \tag{13}$$

$$\beta_\kappa = \frac{3\kappa}{16\pi^2}\,(|\lambda|^2 + |\kappa|^2)\,, \tag{14}$$

$$\beta_{A_\kappa} = \frac{3}{8\pi^2}\,|\lambda|^2\left[|A_\kappa|^2\,|\kappa|^2/|\lambda|^2 + |A_\lambda|\,\cos(\phi_{A_\lambda} - \phi_{A_\kappa})\right]\,, \tag{15}$$

$$\beta_{t_\beta} = \frac{t_\beta}{32\pi^2}\,Y_{t_\beta}\,, \tag{16}$$

$$\beta_{\mu_{\rm eff}} = \mu_{\rm eff}\,(\beta_\lambda/\lambda - \beta_\kappa/(3\kappa))\,, \tag{17}$$

$$Y_\lambda = \sum_{g=1}^{3}\left[3\,Y_{d_g}^2 + 3\,Y_{u_g}^2 + Y_{e_g}^2\right],$$

$$Y_{t_\beta} = \sum_{g=1}^{3}\left[3\,Y_{d_g}^2 - 3\,Y_{u_g}^2 + Y_{e_g}^2\right], \tag{18}$$

$$Y_{d_g} = \frac{e}{\sqrt{2}M_W s_{\rm w} c_\beta}\,m_{d_g}, \quad Y_{u_g} = \frac{e}{\sqrt{2}M_W s_{\rm w} s_\beta}\,m_{u_g},$$

$$Y_{e_g} = \frac{e}{\sqrt{2}M_W s_{\rm w} c_\beta}\,m_{e_g}. \tag{19}$$

Internally in our code as default, $\overline{\rm DR}$ parameters and their corresponding counter terms are used. It should furthermore be noted that the phase of A_κ is left as a free parameter.

The MSSM limit

We define the MSSM-limit of the NMSSM as follows:

$$\lambda \to 0\,, \quad \kappa \to 0 \quad (\text{with} \lambda/\kappa \text{fixed, we choose} \lambda/\kappa = 1)\,, \quad \phi_H \to 0\,, \tag{20}$$

where the latter denotes a possible phase of the second Higgs doublet.

3 Calculation of diagrams

In this section we give some details regarding the calculation of the tree-level and higher-order corrections to the production of the lightest Higgs boson $h_1 \equiv h_{125}$ in e^+e^- collisions, see Eq. 2. The diagrams and corresponding amplitudes have been obtained with `FeynArts` (version 3.11) [98–100], using the (N)MSSM model file[4] (including the (N)MSSM counterterms) of Refs. [28,88]. The further evaluation has been performed with `FormCalc` (version 9.10) and `LoopTools` (version 2.16) [101]. The Higgs masses have been evaluated using the Fortran program `NMSSMCALC` (version 5.0) [81–85] with $\mathcal{O}(\alpha_t\alpha_s + \alpha_t^2)$ two-loop corrections and OS renormalization in the (s)top-sector. Furthermore we use $M_{H^\pm}$ as input parameter and allow for general $\mathcal{CP}$-violation. The numerical input values are given in Sect. 4.1.

3.1 Contributing diagrams

Sample diagrams for the process $e^+e^- \to h_1 Z$ are shown in Fig. 1. Not shown are the diagrams for real (hard and soft) photon radiation. They are obtained from the corresponding tree-level diagrams by attaching a photon to the electrons/positrons. The internal particles in the generically depicted diagrams in Fig. 1 are labeled as follows: F can be a SM fermion f, chargino $\tilde{\chi}_c^\pm$ or neutralino $\tilde{\chi}_n^0$; S can be a sfermion $\tilde{f}_s$ or a Higgs (Goldstone) boson h_i, $H^\pm$ (G, $G^\pm$); U denotes the ghosts u_V; V can be a photon γ or a massive SM gauge boson, Z or $W^\pm$. As the impact of the electron–Higgs coupling on the computed cross-sections is well below the theoretical uncertainty, we have neglected all these couplings via the `FeynArts` command [98–100]

```
Restrictions -> NoElectronHCoupling
```

and terms proportional to the electron mass `ME` (and the squared electron mass `ME2`) via the `FormCalc` command [101]

```
Neglect[ME] = Neglect[ME2] = 0,
```

which allows `FormCalc` to replace `ME` by zero whenever this is safe, i.e. except when it appears in negative powers or in loop integrals. We have verified numerically that these contributions are indeed totally negligible. For internally appearing Higgs bosons no higher-order corrections to their masses or couplings are taken into account; these corrections would correspond to effects beyond one-loop order for the process $e^+e^- \to h_1 Z$.[5] For external Higgs bosons, on-shell (OS) masses (including two-loop corrections at $\mathcal{O}(\alpha_t\alpha_s + \alpha_t^2)$) are used, obtained with `NMSSMCALC` (version 5.0) [81–85].[6]

Also not shown are the wave function correction diagrams with a Z/Goldstone/Higgs–Higgs boson self-energy contribution on the external h_1-boson leg. They appear diagrammatically with a $Z/G/h_i$–h_1 transition ($i = 1, \ldots, 5$).

[4] It should be noted that the NMSSM model file (including the corresponding driver files for `FormCalc`) which we have developed, are not yet officially part of `FeynArts` and `FormCalc`.

[5] We found that using loop corrected Higgs boson masses in the loops leads to a UV divergent result.

[6] We have checked numerically that our results, with (or without) loop corrected *external* Higgs masses, are finite.

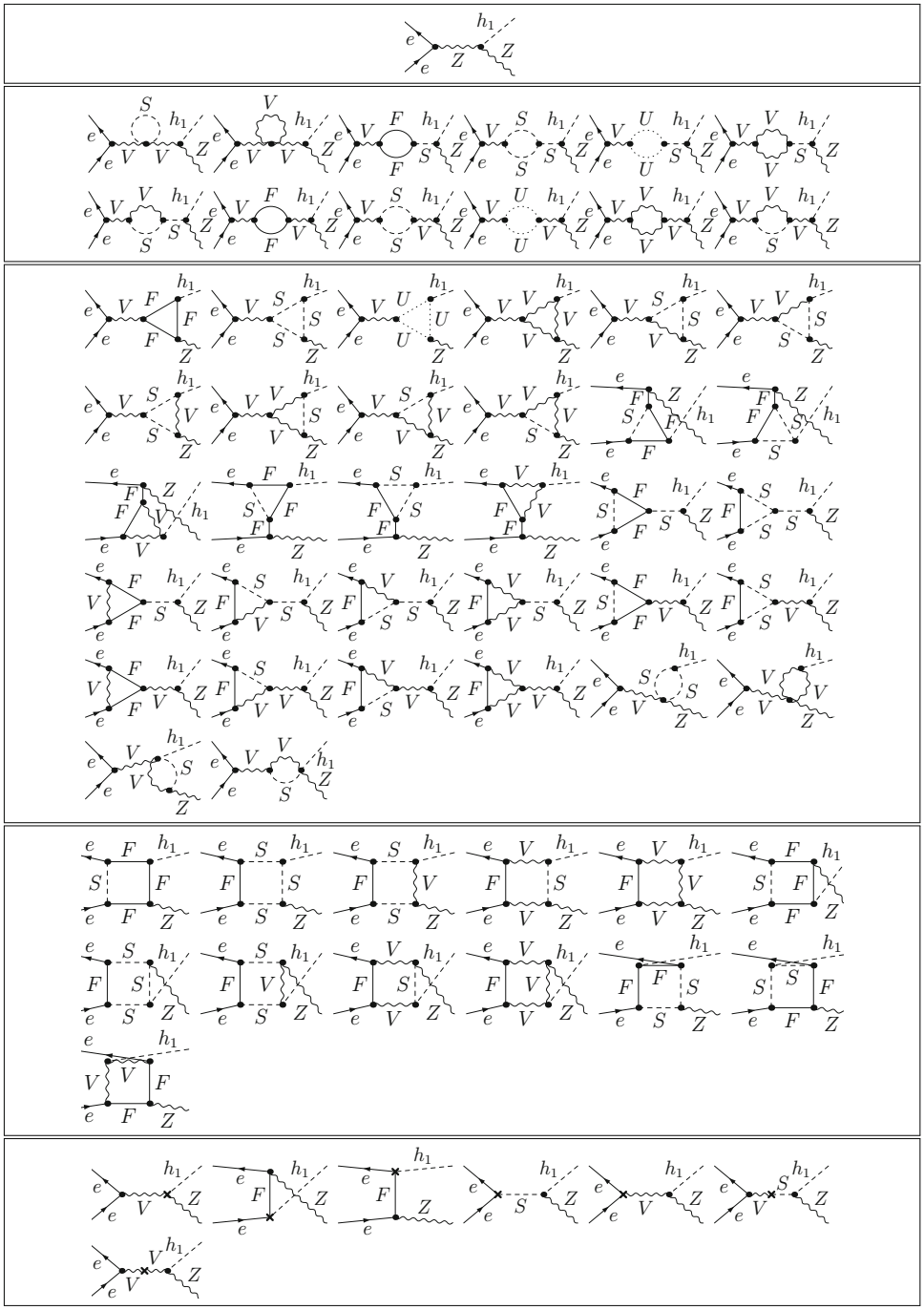

Fig. 1 Generic tree, self-energy, vertex, box, and counterterm diagrams for the process $e^+e^- \to h_1 Z$. F can be a SM fermion, chargino or neutralino; S can be a sfermion or a Higgs/Goldstone boson; V can be a γ, Z or $W^\pm$. It should be noted that electron–Higgs couplings are neglected

The Z/G–h_1 self-energy diagrams belonging to the process $e^+e^- \to Zh_1$, yield a vanishing contribution for external on-shell gauge bosons due to $\epsilon \cdot p = 0$ for $p^2 = M_Z^2$, where p denotes the external momentum and ϵ the polarization vector of the gauge boson. The h_1–h_1-boson transition cannot be taken into account diagrammatically in `FeynArts/FormCalc` because it leads to a division by zero. Furthermore, the h_1–h_i ($i \neq 1$) transition can only be calculated at the `Particles` level in `FeynArts/FormCalc`, leading to 548 diagrams. Therefore we have implemented these self-energies directly via

$$\hat{\Sigma}_{h_1 h_i}(p^2) = -\frac{2}{m_{h_1}^2 - m_{h_i}^2} \left\{ \Sigma_{h_1 h_i}(p^2) + \tfrac{1}{2}\,(m_{h_1}^2 - \bar{m}_{h_1}^2 + m_{h_1}^2 - \bar{m}_{h_i}^2)\,\delta Z_{h_1 h_i} - \delta M_{h_1 h_i} \right\}, \tag{21}$$

with $i \neq 1$ and $\bar{m}_{h_i}$ denotes the tree level Higgs masses, while m_{h_i} denotes the two-loop corrected Higgs masses at $\mathcal{O}(\alpha_t\alpha_s + \alpha_t^2)$, obtained with `NMSSMCALC` (version 5.0) [81–85]. The diagonal contribution, i.e. $i = 1$, is implemented directly by the corresponding limit as (see, e.g. Eq. (49) in [102]),

$$\hat{\Sigma}'_{h_1h_1}(p^2) = -\frac{\partial}{\partial p^2}\Sigma_{h_1h_1}(p^2) - \delta Z_{h_1h_1}. \tag{22}$$

More details on this "limit $i \to 1$" are provided in the Appendix.

Furthermore, in general, in Fig. 1 we have omitted diagrams with self-energy type corrections of external (on-shell) particles. While the contributions from the real parts of the loop functions are taken into account via the renormalization constants defined by OS renormalization conditions, the contributions coming from the imaginary part of the loop functions can result in an additional (real) correction if multiplied by complex parameters. In the analytical and numerical evaluation, these diagrams have been taken into account via the prescription given in [88].

Within our one-loop calculation we neglect finite width effects that can help to cure threshold singularities. Consequently, in the close vicinity of those thresholds our calculation does not give a reliable result. Switching to a complex mass scheme [103] would be another possibility to cure this problem, but its application is beyond the scope of our paper (see also [104] for earlier ideas to address this problem).

For completeness we show here the tree-level cross section formula:

$$\begin{aligned}\sigma_{\text{tree}}(e^+e^- \to h_1 Z) = \frac{\pi\,\alpha^2}{96\,s}\left(\frac{8\,s_{\text{w}}^4 - 4\,s_{\text{w}}^2 + 1}{s_{\text{w}}^4\,c_{\text{w}}^4}\right) \\ \frac{\lambda(1, m_{h_1}^2/s, M_Z^2/s) + 12\,M_Z^2/s}{(1 - M_Z^2/s)^2} \\ \times \quad \lambda^{1/2}(1, m_{h_1}^2/s, M_Z^2/s) \\ \left|c_\beta\, Z_{11}^{\text{mix}} + s_\beta\, Z_{12}^{\text{mix}}\right|^2 ,\end{aligned} \tag{23}$$

where $\lambda(x, y, z) = (x-y-z)^2 - 4yz$ denotes the usual two-body phase space function and Z_{ij}^{mix} denote the coefficients of the transition matrix $\mathbf{Z}^{\text{mix}}$ to the physical Higgs fields, which is further outlined in [28].

3.2 Ultraviolet divergences

As regularization scheme for the UV divergences we have used constrained differential renormalization [105], which has been shown to be equivalent to dimensional reduction [106,107] at the one-loop level [101]. Thus the employed regularization scheme preserves SUSY [108,109] and guarantees that the SUSY relations are kept intact, e.g. that the gauge couplings of the SM vertices and the Yukawa couplings of the corresponding SUSY vertices also coincide to one-loop order in the SUSY limit (i.e. for SUSY masses being equal to their corresponding SM masses). Therefore no additional shifts, which might occur when using a different regularization scheme, arise. All UV divergences cancel in the final result.

3.3 Infrared divergences

Soft photon emission implies numerical problems in the phase space integration of radiative processes. The phase space integral diverges in the soft energy region where the photon momentum becomes very small, leading to infrared (IR) singularities. Therefore the IR divergences from diagrams with an internal photon have to cancel with the ones from the corresponding real soft radiation. We have included the soft photon contribution via the code already implemented in `FormCalc` following the description given in [110]. The IR divergences arising from the diagrams involving a photon are regularized by introducing a photon mass parameter, λ_γ. All IR divergences, i.e. all divergences in the limit $\lambda_\gamma \to 0$, cancel once virtual and real diagrams for one process are added. We have (numerically) checked that our results do not depend on λ_γ.

We have also numerically checked that our results do not depend on $\Delta E = \delta_s E = \delta_s\sqrt{s}/2$ defining the energy cut that separates the soft from the hard radiation. As one can see from the example in the upper plot of Fig. 2 this holds for four orders of magnitude within the numerical accuracy.[7] Our numerical results below have been obtained for fixed $\delta_s = 10^{-3}$.

3.4 Collinear divergences

Numerical problems in the phase space integration of the radiative process arise also through collinear photon emission. Mass singularities emerge as a consequence of the collinear photon emission off massless particles. But already very light particles (such as electrons) can produce numerical instabilities.

There are several methods for the treatment of collinear singularities. In the following, we give a very brief description of the so-called *phase space slicing* (PSS) *method* [111–114], which we adopted in our calculation. The treatment of collinear divergences is not (yet) implemented in `FormCalc`, and therefore we have developed and implemented the code necessary for the evaluation of collinear contributions.

In the PSS method, the phase space is divided into regions where the integrand is finite (numerically stable) and regions where it is divergent (or numerically unstable). In the stable regions the integration is performed numerically, whereas in

[7] It should be noted that for decreasing cuts the integration error roughly grows $\propto \ln(\Delta E/E)$. On the other hand, cuts that are too large or too small lead to manifestly incorrect results.

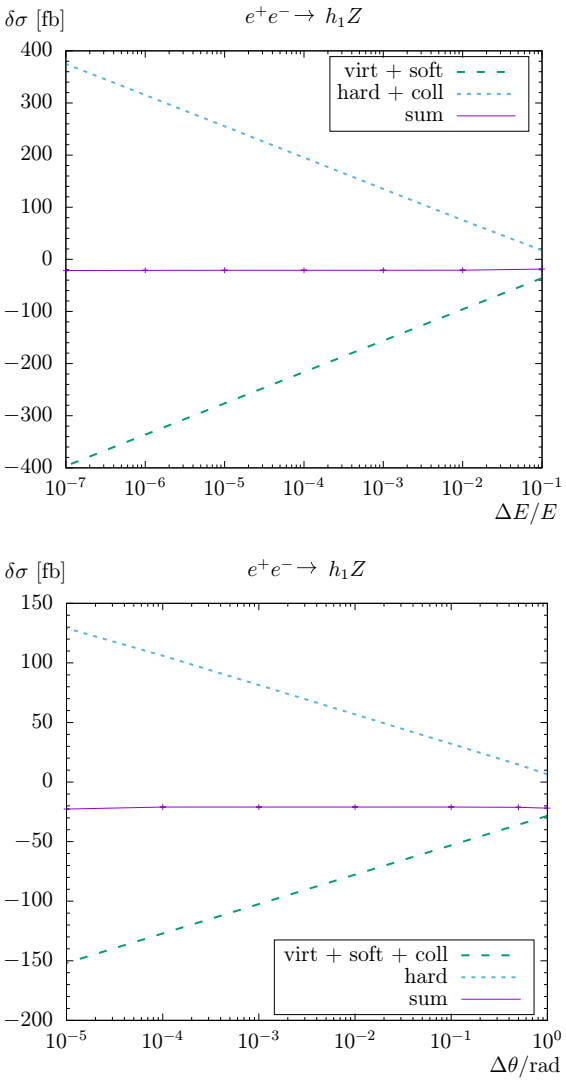

Fig. 2 Phase space slicing method. The different contributions to the loop corrections $\delta\sigma(e^+e^- \to h_1 Z)$ at $\sqrt{s} = 250$ GeV with fixed $\Delta\theta/\text{rad} = 10^{-2}$ (upper plot) and fixed $\Delta E/E = 10^{-3}$ (lower plot)

$\Delta E/E$	$\delta\sigma$/fbarn
10^{-1}	-18.70 ± 0.01
10^{-2}	-20.77 ± 0.03
10^{-3}	-20.94 ± 0.05
10^{-4}	-20.98 ± 0.08
10^{-5}	-21.00 ± 0.10
10^{-6}	-21.12 ± 0.14
10^{-7}	-21.53 ± 0.24

$\Delta\theta$/rad	$\delta\sigma$/fbarn
10^{0}	-21.89 ± 0.03
10^{-1}	-20.94 ± 0.04
10^{-2}	-20.94 ± 0.05
10^{-3}	-20.94 ± 0.08
10^{-4}	-21.00 ± 0.10
10^{-5}	-22.66 ± 0.12

the unstable regions it is carried out (semi-) analytically using approximations for the collinear photon emission [111–114].

The collinear part is constrained by the angular cut-off parameter $\Delta\theta$, imposed on the angle between the photon and the (in our case initial state) electron/positron.

The differential cross section for the collinear photon that is radiated off from the initial state e^+e^- pair corresponds to a convolution

$$\mathrm{d}\sigma_{\text{coll}}(s) = \frac{\alpha}{\pi}\int_0^{1-\delta_s} \mathrm{d}z\, \mathrm{d}\sigma_{\text{tree}}(\sqrt{zs}) \times \left\{\left[2\,\ln\left(\frac{\Delta\theta\sqrt{s}}{2\,m_e}\right) - 1\right] P_{ee}(z) + 1 - z\right\}, \tag{24}$$

with $P_{ee}(z) = (1+z^2)/(1-z)$ denoting the splitting function of a photon from the initial e^+e^- pair. The electron momentum is reduced (because of the radiated photon) by the fraction z such that the center-of-mass frame of the hard process receives a boost. The integration over all possible factors z is constrained by the soft cut-off $\delta_s = \Delta E/E$, to prevent over-counting in the soft energy region.

We have checked (numerically) that our results do not depend on $\Delta\theta$ over four orders of magnitude;[8] see the example in the lower plot of Fig. 2. Our numerical results below have been obtained for fixed $\Delta\theta/\text{rad} = 10^{-2}$.

The one-loop corrections of the differential cross section are decomposed into the virtual, soft, hard, and collinear parts as follows:

$$\mathrm{d}\sigma_{\text{loop}} = \mathrm{d}\sigma_{\text{virt}}(\lambda) + \mathrm{d}\sigma_{\text{soft}}(\lambda, \Delta E) + \mathrm{d}\sigma_{\text{hard}}(\Delta E, \Delta\theta) + \mathrm{d}\sigma_{\text{coll}}(\Delta E, \Delta\theta). \tag{25}$$

The hard and collinear parts have been calculated via the Monte Carlo integration algorithm `Vegas` and `Divonne` as implemented in the `CUBA`, `cuba34` library [115,116] as part of `FormCalc` (with a numerical accuracy of 10^{-3}).

[8] See the previous footnote, but with $\ln(\Delta\theta)$ instead of $\ln(\Delta E/E)$.

3.5 Tests and comparisons

In this section we present some tests and comparisons with results from other papers for light neutral Higgs boson decay and production in e^+e^- collisions.

- We have successfully checked our NMSSM tree-level cross section $\sigma_{\text{tree}}(e^+e^- \to h_1 Z)$ against the analytical formula (23).
- We have checked numerically that the MSSM-limit of the NMSSM (i.e. $\lambda \to 0$, $\kappa \to 0$ with λ/κ fixed (here $\lambda/\kappa = 1$), $\phi_H \to 0$) holds. In particular, we checked that in the MSSM limit our results of [41] were found.
- Furthermore we made some direct comparisons for $h_1 \to \tau^+\tau^-$ with `Mathematica` programs of [28], with full agreement.
- The comparisons for the (light) neutral Higgs boson production within the MSSM can be found in [41].
- In [86] one-loop corrections to the Higgs sector were evaluated in the effective-potential approach, taking into account only (s)quarks of the third generation. The corresponding mixing was introduced into the effective ZZh_1 coupling. Furthermore they used a different input scheme and showed only scatter plots with $\sigma_0(hZZ) = \max[\sigma(m_{h_1}), \sigma(m_{h_2}), \sigma(m_{h_3}), \sigma(m_{h_4}), \sigma(m_{h_5})]$, denoting the largest cross section among the five neutral Higgs bosons.
  The level of agreement of such a comparison depends on the correct transformation of the input scheme from our renormalization scheme into the schemes used in [86], as well as on the differences in the employed renormalization schemes as such. In view of the different schemes and the non-trivial conversions such transformations and/or change of our renormalization prescription is beyond the scope of our paper. Furthermore, the fact that the results in [86] are only presented in scatter plots, renders a comparison unfeasible.
- In [87] only tree-level results (in scatter plots) are shown for the NMSSM, rendering a comparison unnecessary.

To our knowledge, there are no other papers dealing with (light) Higgs boson production in e^+e^- collisions within the NMSSM at the *full* one-loop level.

4 Numerical analysis

In this section we present our numerical analysis of light neutral Higgs boson production at e^+e^- colliders in the Higgs-strahlung channel in the c(N)MSSM. In the various figures below we show the cross sections at the tree level ("tree") and at the full one-loop level ("full").

4.1 Parameter settings

The renormalization scale μ_R has been set to the center-of-mass energy, $\sqrt{s}$. The SM parameters are chosen as follows; see also [117]:

- Fermion masses (on-shell masses, if not indicated differently):

$$\begin{aligned} m_e &= 0.51099895\ \text{MeV}, & m_{\nu_e} &= 0, \\ m_\mu &= 105.6583755\ \text{MeV}, & m_{\nu_\mu} &= 0, \\ m_\tau &= 1776.86\ \text{MeV}, & m_{\nu_\tau} &= 0, \\ m_u &= 71.8689\ \text{MeV}, & m_d &= 71.8689\ \text{MeV}, \\ m_c &= 1.27\ \text{GeV}, & m_s &= 93.40\ \text{MeV}, \\ m_t &= 172.69\ \text{GeV}, & m_b &= 4.18\ \text{GeV}. \end{aligned} \tag{26}$$

  According to [117], m_s is an estimate of a so-called "current quark mass" in the $\overline{\text{MS}}$ scheme at the scale $\mu \approx 2$ GeV. $m_c \equiv m_c(m_c)$ and $m_b \equiv m_b(m_b)$ are the "running" masses in the $\overline{\text{MS}}$ scheme. m_u and m_d are effective parameters, calculated through the hadronic contributions to

$$\Delta\alpha^{(5)}_{\text{had}}(M_Z) = \frac{\alpha}{\pi} \sum_{f=u,c,d,s,b} Q_f^2 \left(\ln \frac{M_Z^2}{m_f^2} - \frac{5}{3} \right) \approx 0.02768\,. \tag{27}$$

- Gauge-boson masses:

$$M_Z = 91.1876\ \text{GeV}, \quad M_W = 80.377\ \text{GeV}. \tag{28}$$

- Coupling constants:

$$\alpha(0) = 1/137.03599918\,, \alpha^{\overline{\text{MS}}}(M_Z) = 1/127.951, \quad \alpha_s^{\overline{\text{MS}}}(M_Z) = 0.1179\,. \tag{29}$$

The Higgs masses have been evaluated using `NMSSMCALC` (version 5.0) [81–85]. For the corresponding MSSM masses the MSSM limit of the NMSSM is evaluated.

The SUSY parameters are chosen according to Table 1. This scenario constitutes a viable parameter set for the process $e^+e^- \to h_1 Z$ in the c(N)MSSM. We do not strictly demand that the lightest Higgs boson has a mass around 125 ± 1.5 GeV, although for parts of the parameter space shown in our plots below this is given. This is illustrated in Fig. 3, where we show m_{h_1} as a function of $|\lambda|$ (left) and $|\kappa|$ (right) in our scenario. One can observe that $m_{h_1} \sim 125$ GeV for $0 \leq |\lambda| \lesssim 0.3$ and $|\kappa| \gtrsim 0.4$, where the actual values of $|\lambda|$ and $|\kappa|$ are indicated by vertical lines. Consequently, these ranges can be seen as in agreement with the experimental measurements. These ranges can vary if other parameters that

Table 1 NMSSM default input parameters in $\overline{\text{DR}}$ at the scale m_t for the numerical investigation and the corresponding Higgs masses; all parameters (except of $t_\beta, \lambda, \kappa, \phi_H$) are in GeV. Calculated masses (values) are rounded to 1 MeV (10^{-3}). Also shown are the input parameters converted to the scale $Q = m_{h_1} + M_Z$. The values for the trilinear sfermion Higgs couplings, A_f are chosen such that charge- and/or color-breaking minima are avoided [118–124], with $A_{f\neq t} = 0$. It should be noted that for the first and second generation of sfermions we chose instead $M_{\tilde{Q},\tilde{U},\tilde{D}} = 3000$ GeV. The phases of the potential complex parameters are zero in our benchmark scenario, i.e. $\varphi_\lambda = \varphi_\kappa = \varphi_{\mu_{\text{eff}}} = \varphi_{A_\kappa} = \varphi_{A_t} = 0$. $M_{h,H,A}$ denote the Higgs-boson masses. ZZh_1 is the Z-Z-Higgs coupling in the NMSSM; ZZh is the corresponding MSSM-limit, given by $ZZh = \frac{e\, M_W\, s_{\beta-\alpha}}{c_w^2\, s_w}$. $c_\beta\, Z_{11}^{\text{mix}} + s_\beta\, Z_{12}^{\text{mix}}$ is the "NMSSM equivalent" of $s_{\beta-\alpha}$ in the MSSM

$\sqrt{s}$	sgn(A_κ)	ϕ_H	$M_{H^\pm}$	$M_{\tilde{Q}_3,\tilde{U}_3,\tilde{D}_3}$	$M_{\tilde{L},\tilde{E}}$	$\lvert A_t\rvert$	M_1	M_2	M_3
250	−1	0	1000	1500	1000	2000	600	400	2500

Scale	$\lvert\lambda\rvert$	$\lvert\kappa\rvert$	$\lvert A_\kappa\rvert$	t_β	$\lvert\mu_{\text{eff}}\rvert$
m_t	0.250	0.480	300.000	7.000	300.000
Q	0.251	0.481	301.299	6.972	300.754

Scale	m_{h_1}	m_{h_2}	m_{h_3}	m_{h_4}	m_{h_5}	ZZh_1	$c_\beta\, Z_{11}^{\text{mix}} + s_\beta\, Z_{12}^{\text{mix}}$
m_t	125.084	728.972	992.400	1000.919	1085.863	66.327472	0.99992867
Q	125.072	731.186	992.457	1000.985	1087.438	66.327470	0.99992865

Scale	M_h	M_H	M_A	ZZh	$s_{\beta-\alpha}$
m_t	125.062	996.828	996.575	66.332033	0.99999743
Q	125.043	996.831	996.575	66.332031	0.99999742

have a large impact on the prediction of m_{h_1} (such as A_t) are varied. Also shown is the value of M_h in the MSSM that has been obtained in the MSSM limit of the NMSSM result (see the discussion above) and is found to be $M_h \approx 125.05$ GeV.

Furthermore, in our baseline scenario one finds $h_1 \sim h$, and since the ZZh coupling in the MSSM is $\propto s_{\beta-\alpha} \to 1$ in the decoupling limit, relatively large cross sections are found. This, however, can be different for the variation of the baseline scenario. We will show the variation with respect to $\sqrt{s}$, $|\lambda|$, $|\kappa|$, $|\mu_{\text{eff}}|$, $M_{H^\pm}$, $M_{\tilde{Q}_3}$, $M_{\tilde{U}_3}$, $|A_\kappa|$, A_t and t_β. as well as the phases of the complex parameters, φ_λ, φ_κ, $\varphi_{\mu_{\text{eff}}}$, and φ_{A_t}, the phase of A_t.

When performing an analysis involving complex parameters it should be noted that the results for physical observables are affected only by certain combinations of the phases of the parameters μ, the trilinear couplings A_f and the gaugino mass parameters $M_{1,2,3}$ [125,126]. For simplicity, we chose to vary the phases of λ, κ, μ_{eff} and A_t independently.

The numerical results shown in the next subsections are of course dependent on the choice of the SUSY parameters. Nevertheless, they give an idea of the relevance of the full one-loop corrections.

4.2 The process $e^+e^- \to h_1 Z$ in the (N)MSSM

The results shown in this and the following subsection consist of "tree", which denotes the tree-level value, and of "full", which is the cross section including *all* one-loop corrections as described in Sect. 3. All these processes are of particular interest for all proposed future e^+e^- colliders (as emphasized in Sect. 1). All calculations have been performed using the $\overline{\text{DR}}$ scale $Q = m_{h_1} + M_Z$.

4.2.1 Full one-loop results for varying real parameters

We begin the numerical analysis with the cross sections of $e^+e^- \to h_1 Z$ evaluated as a function of the real parameters in the NMSSM. In Figs. 4, 5, fig:eeh1Zsps3 and 7 we show the results for the process $e^+e^- \to h_1 Z$ in the (N)MSSM, as a function of $\sqrt{s}$, $|\lambda|$, $|\kappa|$, $|\mu_{\text{eff}}|$, $M_{H^\pm}$, $M_{\tilde{Q}_3}$, $M_{\tilde{U}_3}$, $|A_\kappa|$, A_t and t_β, respectively.

We start with the process $e^+e^- \to h_1 Z$ for the parameters given in Table 1 as a function of $\sqrt{s}$ as shown in the upper part of Fig. 4. The total cross section starts at the production threshold $m_{h_1} + M_Z = 216.260$ GeV. At the tree-level one finds a maximum of about 203 fb in the (N)MSSM at $\sqrt{s} \approx 255$ GeV with a decrease for increasing $\sqrt{s}$. The results of the NMSSM are effectively indistinguishable from the MSSM. The size of the corrections to the cross section (upper right plot in Fig. 4) can be especially large in close vicinity to the production threshold[9] from which on the considered process is kinematically possible. At the production threshold we found relative corrections (i.e. $\sigma_{\text{loop}}/\sigma_{\text{tree}}$) of $\approx -30\%$. Away

[9] It should be noted that a calculation very close to the production threshold requires the inclusion of additional (nonrelativistic) contributions, as well as resummation of soft-photon effects, which is beyond the scope of this paper. Consequently, very close to the production threshold our calculation (at the tree and loop level) does not provide a very accurate description of the cross section.

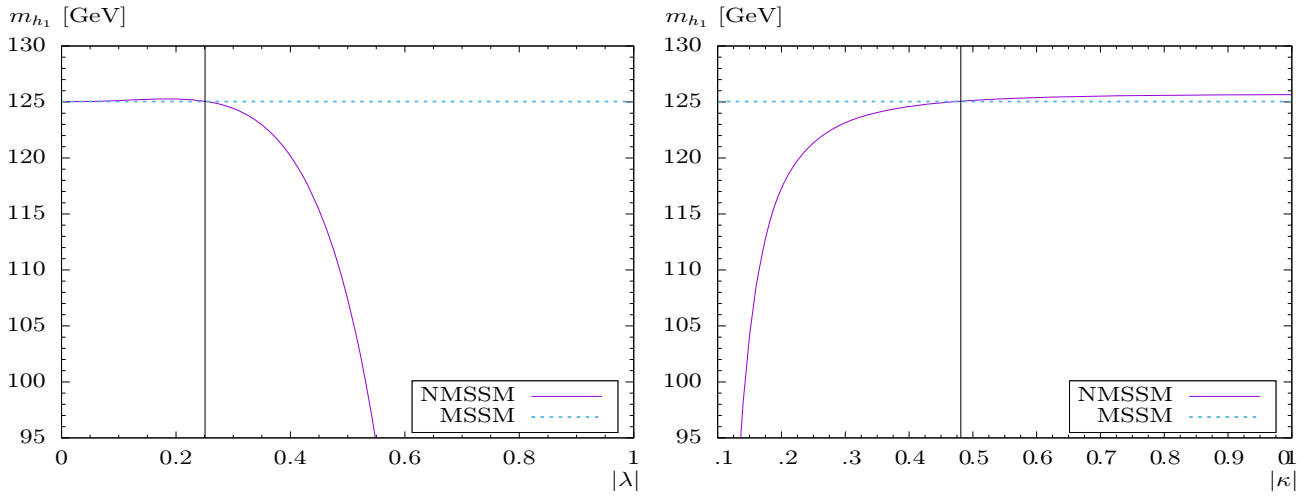

Fig. 3 The light Higgs boson masses of the NMSSM and MSSM are shown with $|\lambda|$ varied (left) and $|\kappa|$ varied (right). The thin black lines cross with the purple solid and blue dotted lines in our default parameter point, see Table 1

from the production threshold, loop corrections of $\approx -10\%$ at $\sqrt{s} = 250$ GeV are found, increasing to $\approx +22\%$ at $\sqrt{s} = 1000$ GeV. The very small dip at $\sqrt{s} \approx 545$ GeV is the chargino production threshold $\sqrt{s} = m_{\tilde{\chi}_1^\pm} + m_{\tilde{\chi}_1^\pm}$ (see the inlay in the plot).

Also at the one-loop level the deviation of $\sigma_{\text{loop}}/\sigma_{\text{tree}}$ between the NMSSM and MSSM is extremely small, i.e. the loop corrections do not differ in a relevant way due to the extended NMSSM particle spectrum. It should be noted that this equality crucially depends on the fact that the scenario results in effectively identical light Higgs boson masses in the two models, see Table 1.

Following the running scenarios of the proposed future e^+e^- colliders, supported by the location of the maximum cross sections discussed above, in the following plots we always assume $\sqrt{s} = 250$ GeV.

In the lower part of Fig. 4 the cross section is analyzed in dependence of $|\lambda|$.[10] The left plot shows the cross section starting at $|\lambda| = 0.01$. (We cannot start directly at zero, because a negative eigenvalue in the loop Higgs mass matrix of NMSSMCALC appears for $|\lambda| < 0.007$, due to a numerical instability. But the MSSM limit input (i.e. Eq. 20) for NMSSMCALC avoids this numerical instability.) The part of the parameter space where m_{h_1} deviates more than about 1.5 GeV from M_h, see Fig. 3, is shaded in gray. As an example, starting from $|\lambda| \approx 0.3$ the NMSSM cross section strongly increases up to 325 fb at $|\lambda| \approx 0.55$, where $m_{h_1} = 93.65$ GeV. Consequently, this increase is a pure kinematic effect. The relative corrections, as shown in the lower right plot, are nearly constant in the allowed parameter space and reach $\approx -9.5\%$. The MSSM limit is constant (because $\lambda \equiv 0$) at 202 fb and the relative correction is found to be effectively identical to the NMSSM.

In Fig. 5 we analyze the cross section in dependence of $|\kappa|$ (upper row) and $|\mu_{\text{eff}}|$ (lower row). In the upper left plot we start at $|\kappa| \approx 0.13$ because $m_{h_1}^2 < 0$ for lower values. The excluded region for $m_{h_1} < 123.5$ GeV is in light-gray. Again the MSSM limit is constant due to $\kappa \equiv 0$ at 202 fb, and the relative correction is about -9.5%, as in the case of the $|\lambda|$ variation. The maximum deviation of the relative corrections between the NMSSM and MSSM amounts only to 0.64% at $|\kappa| \approx 0.31$. However, these small differences of up to ~ 5 fb can be attributed to the deviation between m_{h_1} and M_h reaching 1.5 GeV.

In the lower left plot the NMSSM cross section is shown as a function of $|\mu_{\text{eff}}|$, starting at ≈ 105 GeV because $m_{\tilde{\chi}_1^\pm} < 94$ GeV (the lower limit for $|\mu_{\text{eff}}| < 103$ GeV in our scenario). The light-gray (dark-gray) areas are excluded by $m_{h_1} < 123.5$ GeV ($M_h < 123.5$ GeV). The thin black solid line indicates $m_{h_1} \approx M_h \approx 125$ GeV. The NMSSM cross section reaches a minimum of 198 fb at $\mu_{\text{eff}} \approx 155$ GeV and slightly increases with increasing μ_{eff}. A smaller increase is visible also for the MSSM results, and the small deviations between the NMSSM and MSSM cross sections, reaching ± 5 fb, can again be attributed to changes in m_{h_1} of up to ± 1.5 GeV. The relative corrections (lower right plot) in the (N)MSSM reach about -10.5% in the respective minimum. The maximum deviation of the relative corrections between the NMSSM and MSSM is (in the allowed region) 0.4% at $|\mu_{\text{eff}}| \approx 1203$ GeV, effectively due to the change in m_{h_1}.

In the upper left plot of Fig. 6 we show the (N)MSSM cross sections as a function of $M_{H^\pm}$. As before the regions with $m_{h_1} < 123.5$ GeV are light gray shaded, where the left shaded area is also valid for the MSSM. Overall, the

[10] Here and in the following we denote the potentially complex parameters z as $|z|$, keeping in mind that in the benchmark scenario we have defined $\varphi_z = 0$. We specify explicitely when we deviate from $\varphi_z = 0$.

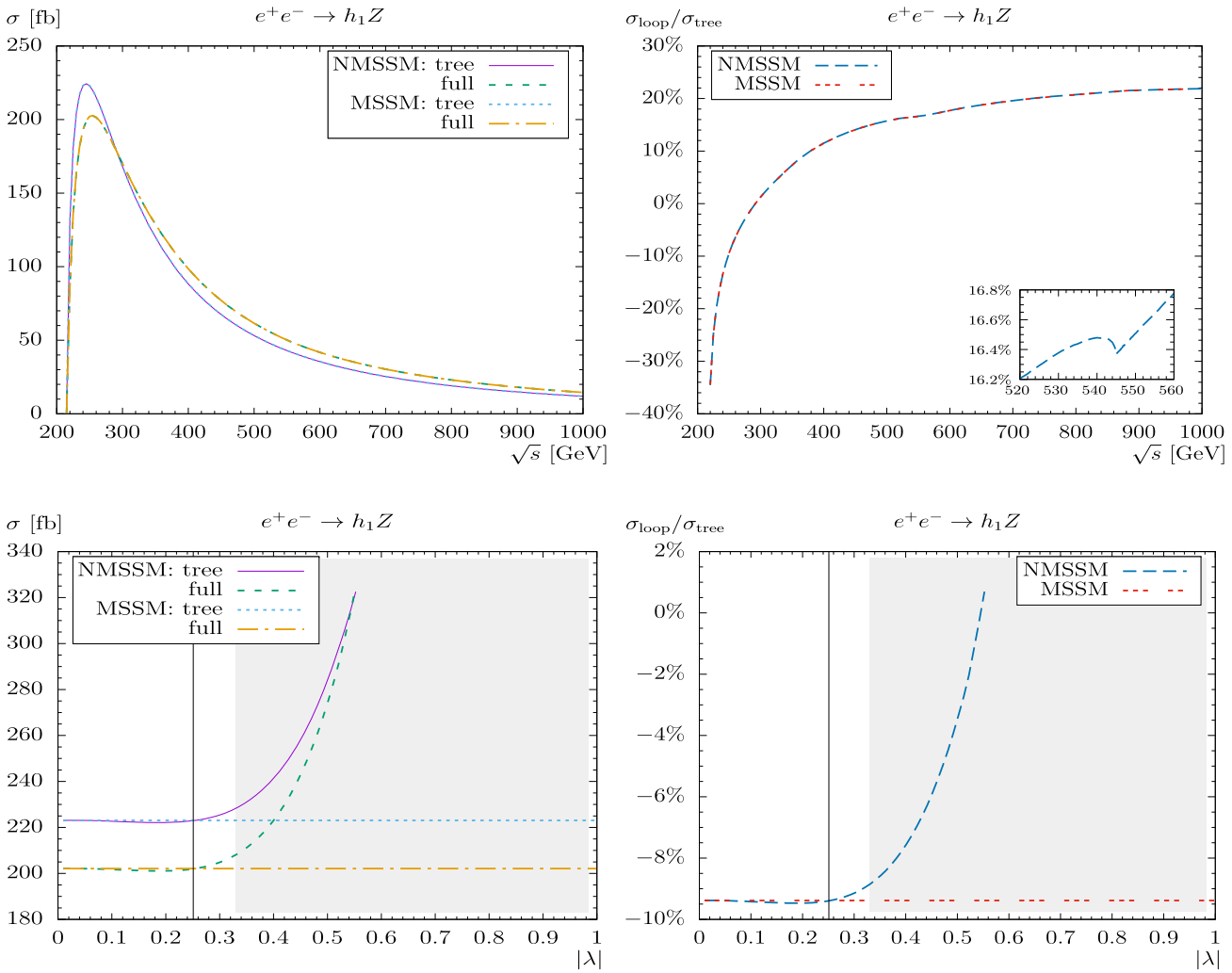

Fig. 4 $\sigma(e^+e^- \to h_1 Z)$. Tree-level and full one-loop corrected cross sections in the (N)MSSM are shown with parameters chosen according to Table 1. The upper plots show the cross sections with $\sqrt{s}$ varied (left) and the corresponding $\sigma_{\text{loop}}/\sigma_{\text{tree}}$ in percent (right); the lower plots show $|\lambda|$ varied (left) and the corresponding $\sigma_{\text{loop}}/\sigma_{\text{tree}}$ in percent (right). The gray area is excluded by $m_{h_1} < 123.5$ GeV. The thin black solid line indicates $m_{h_1} \approx M_h \approx 125$ GeV. It should be noted, that $\lambda \equiv 0$ in the MSSM limit, therefore here the MSSM cross section is constant

cross section is nearly constant, with a small variation due to the change in m_{h_1} or M_h. The NMSSM loop corrections are mostly at the level of -9.5% in the allowed area, with a similar result for the MSSM. The maximum deviation of the relative corrections between the NMSSM and MSSM amounts to $\approx 0.2\%$ at 1800 GeV.

The effects of $M_{\tilde{Q}_3}$ and $M_{\tilde{U}_3}$, shown in the middle and lower plots of Fig. 6, respectively, are quite similar, and we restrict ourselves to describing the first of this soft breaking parameters. Different values for $M_{\tilde{U}_3}$ are given in brackets. Here, the gray shaded area indicates $m_{h_1} \approx M_h < 123.5$ GeV, where the two Higgs-boson masses exhibit the same dependence on the soft SUSY-breaking parameters in the stop sector. The cross sections start at 1380 GeV because lower values violate the lower bound of $m_{\tilde{t}_1} < 1310$ GeV. The (unusual) very small kink at $M_{\tilde{Q}_3} \approx 2766$ GeV is caused by the loop corrected Higgs masses from NMSSMCALC (see the inlay in the plot). The cross section is found to vary at the level of ± 5 fb, following the change in the light Higgs-boson masses and partially due to genuine scalar top loops in the production cross section. The loop corrections amount to $\approx -8.7\,(8.8)\%$ to $\approx -9.4\%$ for the (N)MSSM. The deviation of the relative corrections between the NMSSM and MSSM is negligibly small.

In the upper row of Fig. 7 we show the dependence of the Higgs-boson production cross sections on $|A_\kappa|$. Here it should be noted that $M_{H^\pm}$ is one of our input parameters and thus remains fixed when $|A_\kappa|$ is varied. As before, the light gray region is excluded by $m_{h_1} < 123.5$ GeV. The full MSSM cross section is constant in the allowed param-

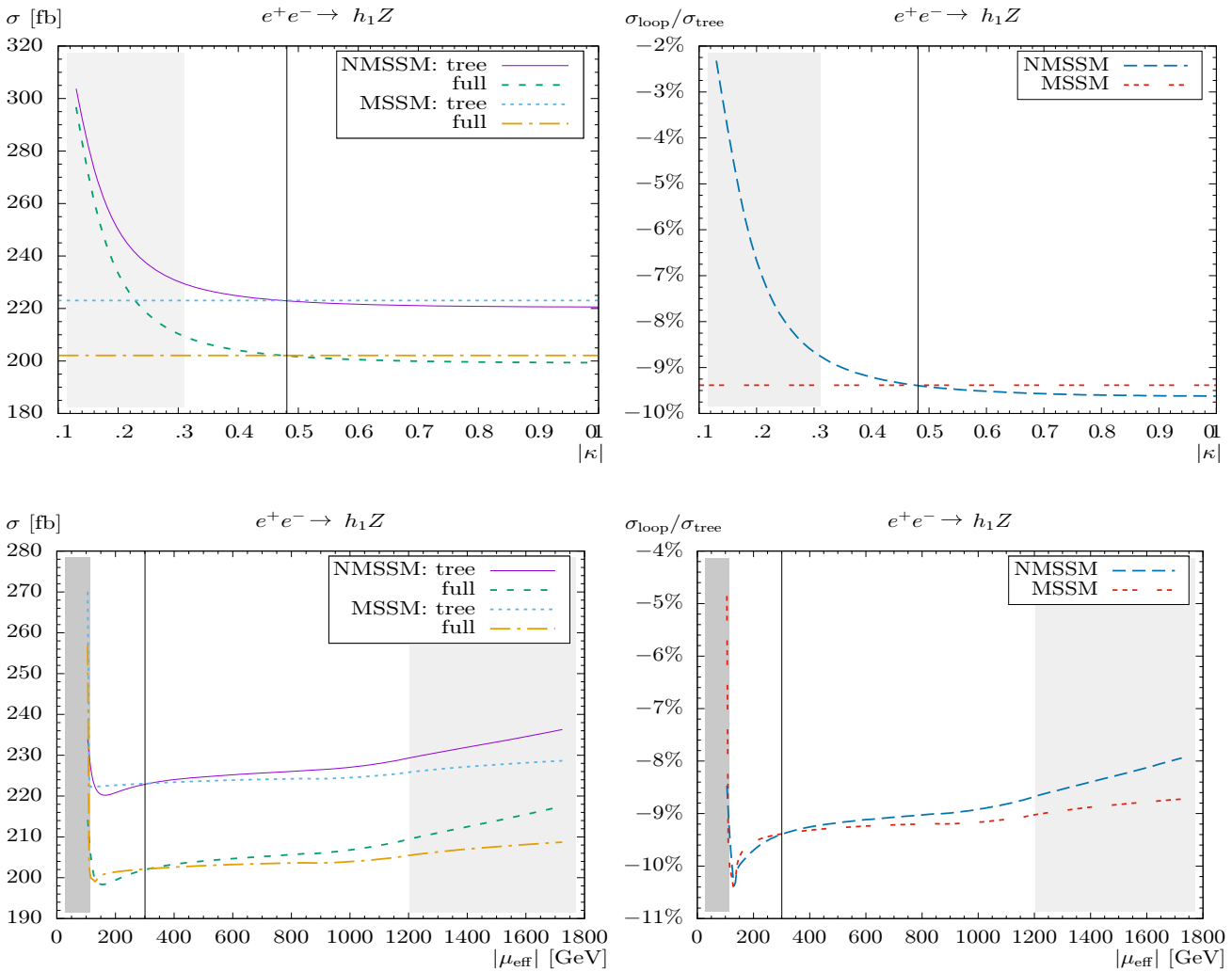

Fig. 5 $\sigma(e^+e^- \to h_1 Z)$. Tree-level and full one-loop corrected cross sections in the (N)MSSM are shown with parameters chosen according to Table 1. The upper plots show the cross sections with $|\kappa|$ varied (left) and the corresponding $\sigma_{\text{loop}}/\sigma_{\text{tree}}$ in percent (right). It should be noted, that $\kappa \equiv 0$ in the MSSM limit, therefore, here the MSSM cross section is constant. The lower plots show μ_{eff} varied (left) and the corresponding $\sigma_{\text{loop}}/\sigma_{\text{tree}}$ in percent (right). The light-gray (dark-gray) areas are excluded by $m_{h_1} < 123.5$ GeV ($M_h < 123.5$ GeV). The thin black solid line indicates $m_{h_1} \approx M_h \approx 125$ GeV

eter space at 222 fb, with an extremely small variation of the NMSSM cross section at larger values of $|A_\kappa|$. The relative corrections (upper right plot) can reach $\approx -9.4\%$ in the allowed region, for both the MSSM and NMSSM. The deviation of the relative corrections between the NMSSM and MSSM reach only 0.14%.

The variation of the cross sections with A_t is shown in the middle plots of Fig. 7, with the gray area excluded by $m_{h_1} \approx M_h < 123.5$ GeV. First it should be noted that a numerical instability around -400 GeV (not shown in the plot) is caused by the loop corrected Higgs masses from NMSSMCALC through an internal conversion from $A_t^{\overline{\text{DR}}}$ to A_t^{OS}, which does not converge properly. Therefore a simplified conversion (i.e. no iteration) is used automatically by NMSSMCALC. The cross section follows the mass dependence allowed by the ± 1.5 GeV uncertainty around 125 GeV, where the lowest cross section is reached for the highest Higgs-boson mass of ~ 125 GeV, indicated by the vertical black line. For lower or higher A_t values the Higgs-boson mass goes down, and the cross section rises accordingly, i.e. the variation is a pure artefact of the change in $m_{h_1} \approx M_h$. The loop corrections in the allowed interval are about -9.5% in both models, see the middle right plot. The deviation of the relative corrections between the NMSSM and MSSM is negligible.

Finally, the dependence on t_β is shown in the lower plots of Fig. 7. The NMSSM loop corrections can reach $\approx -9.5\%$ at $t_\beta = 13$, while the MSSM loop corrections reach $\approx -10.3\%$

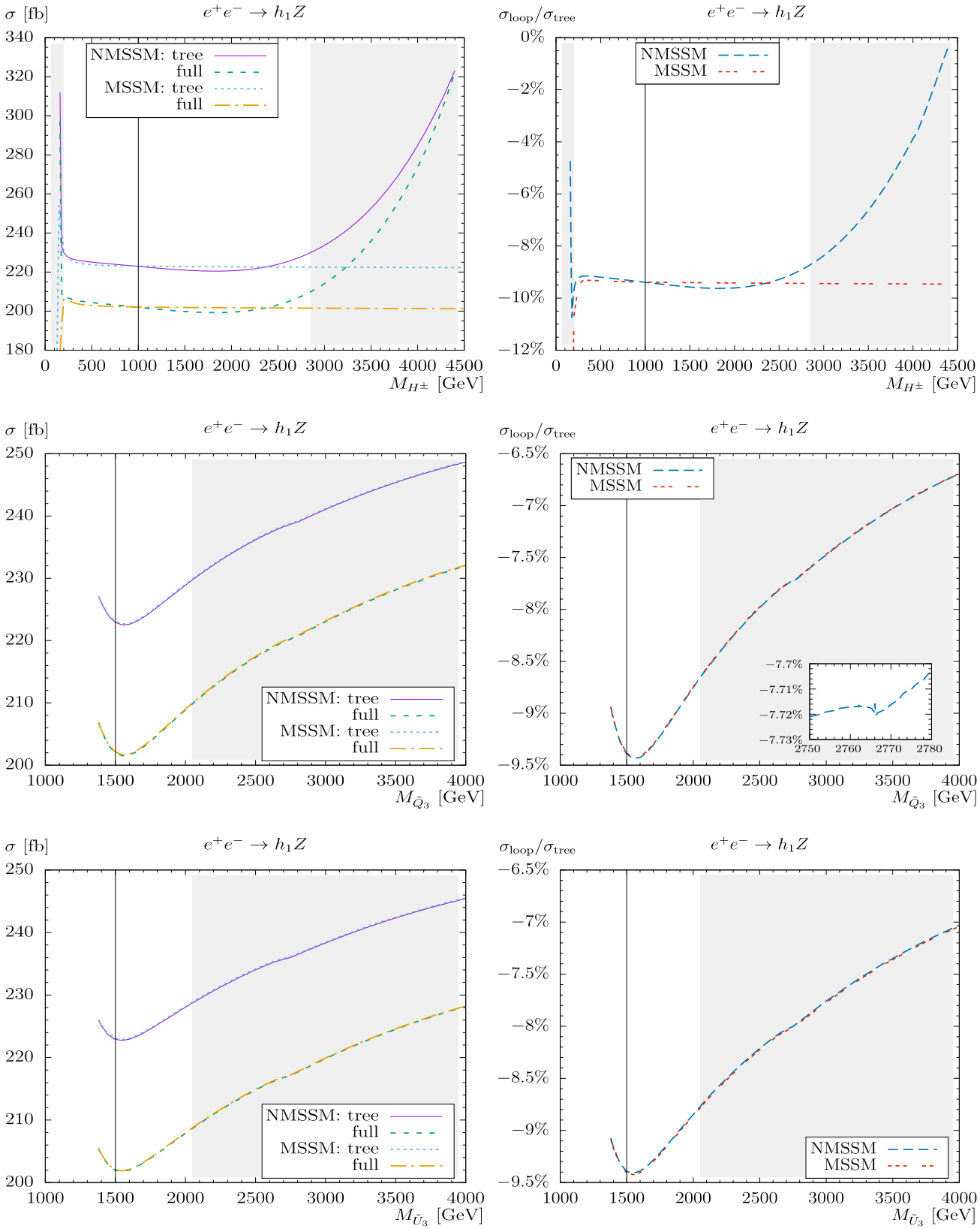

Fig. 6 $\sigma(e^+e^- \to h_1 Z)$. Tree-level and full one-loop corrected cross sections in the (N)MSSM are shown with parameters chosen according to Table 1. The upper plots show the cross sections with $M_{H^\pm}$ varied (left) and the corresponding $\sigma_{\text{loop}}/\sigma_{\text{tree}}$ in percent (right). The middle plots show the cross sections with $M_{\tilde{Q}_3}$ varied (left) and the corresponding $\sigma_{\text{loop}}/\sigma_{\text{tree}}$ in percent (right). The lower plots show $M_{\tilde{U}_3}$ varied (left) and the corresponding $\sigma_{\text{loop}}/\sigma_{\text{tree}}$ in percent (right). The light-gray area is excluded by $m_{h_1} \approx M_h < 123.5$ GeV. The thin black solid line indicates $m_{h_1} \approx M_h \approx 125$ GeV

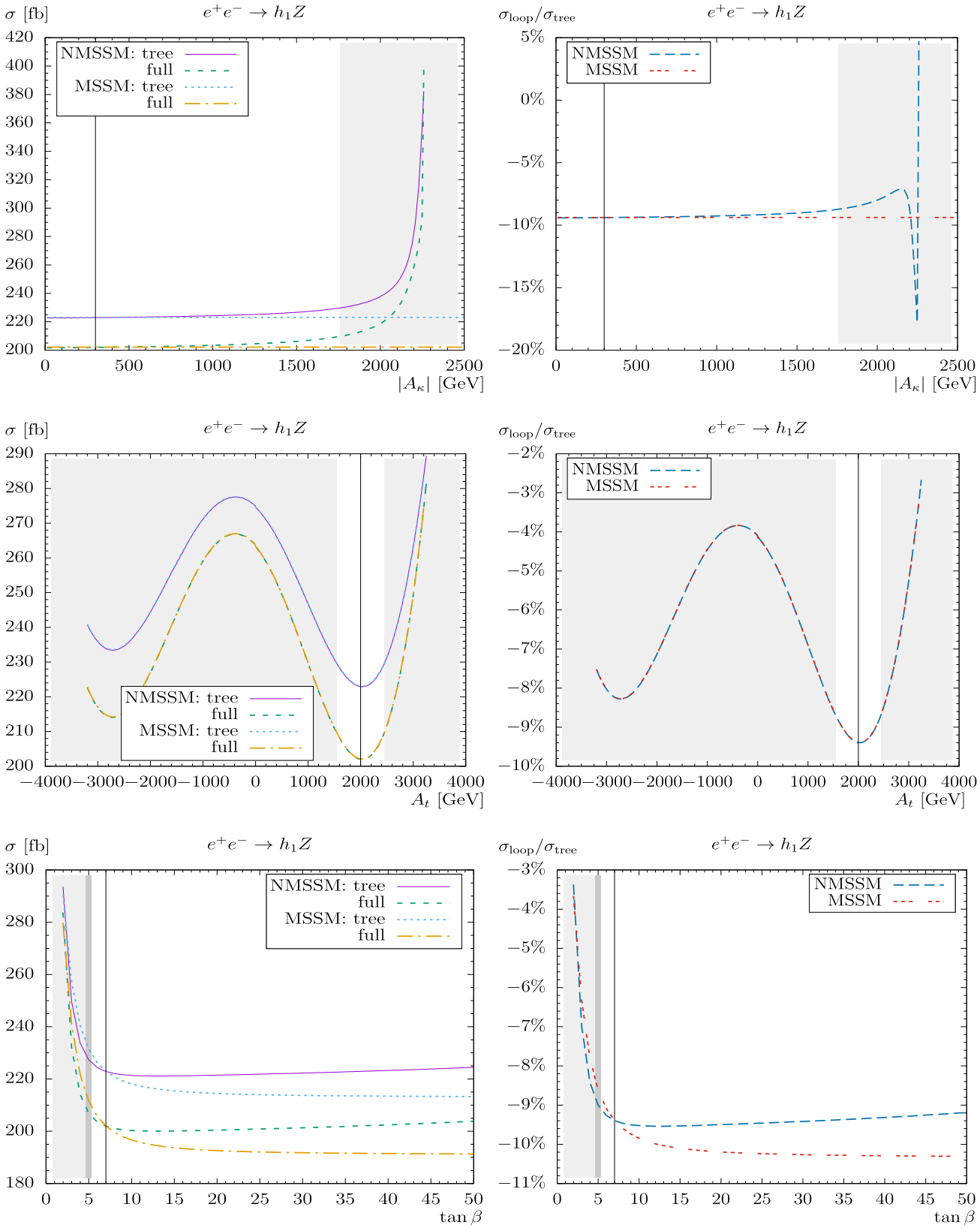

Fig. 7 $\sigma(e^+e^- \to h_1 Z)$. Tree-level and full one-loop corrected cross sections in the (N)MSSM are shown with parameters chosen according to Table 1. The upper plots show the cross sections with $|A_\kappa|$ varied (left) and the corresponding $\sigma_{\text{loop}}/\sigma_{\text{tree}}$ in percent (right). The middle plots show the cross sections with A_t varied (left) and the corresponding $\sigma_{\text{loop}}/\sigma_{\text{tree}}$ in percent (right). The lower plots show t_β varied (left) and the corresponding $\sigma_{loop}/\sigma_{tree}$ in percent (right). The light-gray (dark-gray) area is excluded by $m_{h_1} < 123.5$ GeV ($M_h < 123.5$ GeV). The thin black solid line indicates $m_{h_1} \approx M_h \approx 125$ GeV

at $t_\beta = 50$. The maximum deviation of the relative corrections between the NMSSM and MSSM reach $\approx 1.1\%$ at $t_\beta = 50$, which is (as before) a pure kinematic effect because of the different light Higgs masses.

Overall, we observe that the prediction of the light Higgs-boson production cross section in the NMSSM is nearly indistinguishable from the MSSM cross section. Nearly all (small) observed effects are kinematic, originating from the small variation allowed in m_{h_1} due to the theoretical uncertainties, see [30]. However, since the value of the Higgs-boson mass is determined experimentally to a high accuracy, these kinematic effects must be considered numerical artefacts. The main genuine loop effects of the NMSSM and the MSSM were observed at the percent level in the dependence on $M_{\tilde{Q}_3}$, $M_{\tilde{U}_3}$ and A_t, where the differences between the NMSSM and the MSSM are negligibly small.

4.2.2 *Full one-loop results for varying phases*

We finish the numerical analysis with the cross sections of $e^+e^- \to h_1 Z$ evaluated as a function of the phases of two (potentially) complex parameters in the (N)MSSM: φ_λ, φ_κ, as well as $\varphi_{\mu_{\text{eff}}}$ and φ_{A_t} (all between 0° and 360°). As already emphasized, λ and κ are zero in the MSSM limit, therefore the MSSM cross section is constant.

In the upper left plot of Fig. 8 the dependence of the Higgs-boson production cross section in the (N)MSSM on φ_λ is depicted. Overall a relevant variation can be observed. This occurs, however, mostly in the light gray region with $m_{h_1} < 123.5$ GeV. As in the previous section the variation of the cross section is mainly a kinematic effect due to the "allowed" variation of m_{h_1}. The size of the loop corrections, as before, is found at the level of about -9.5%, see the upper right plot in Fig. 8. Peaks and dips around 30°, 90°, 150°, 210°, 270°, and 330° in φ_λ (not shown in the plot) are due to $m^2_{h_1} < 0$ produced by NMSSMCALC, already at the tree level.[11]

In the middle left plot of Fig. 8 the (N)MSSM cross sections are shown in dependence of φ_κ. As for the dependence on φ_λ, the visible effects are of pure kinematical nature, as can be seen in the comparison to the φ_κ-independent cross sections in the MSSM. The size of the loop corrections stays at the level of about -9.5%, see the middle right plot of Fig. 8. The dependence on ϕ_H is nearly identical, as shown in the lower row of Fig. 8.

We turn to the variation of the Higgs-boson production cross sections with $\varphi_{\mu_{\text{eff}}}$ and φ_{A_t}. The former dependence is shown in the upper plots of Fig. 9. As in the two previous cases, only a variation due to "allowed" variations in m_{h_1} can be observed. The loop corrections stay at the level of about -9.5%, see the upper right plot of Fig. 9. The maximum deviation of the relative corrections between the NMSSM and MSSM reach only 0.6% at these four points.

Finally, the full (N)MSSM cross section for φ_{A_t} is presented in the lower plots of Fig. 9: the results for the two models appear indistinguishable. As for the variation with $|A_t|$, also for the variation of φ_{A_t} no genuine effect beyond $m_{h_1} \approx M_h$ was observed (see also Fig. 7). As before, the size of the loop corrections is found at the level of -9.5% as can be seen in the lower right plot of Fig. 9.

Lastly, a comment on NMSSMCALC is in order. To check whether all the issues we mentioned above are due to NMSSMCALC, we used our own routines restricted to one-loop corrected Higgs masses (instead of the 2-loop corrected by NMSSMCALC). We find that none of the mentioned issues appear in this case. But for our numerical analysis, we have to stick to the substantially more precise two-loop result by NMSSMCALC.

4.2.3 *Summary*

The process $e^+e^- \to h_1 Z$ is of particular interest for colliders operating at $\sqrt{s} = 250$ GeV [31–39], but our results can be taken over to higher energies as well [36–40]. The precise prediction of the production cross section is crucial for an accurate determination of the Higgs-boson couplings to SM fermions and gauge bosons. In our numerical analysis we have demonstrated that the one-loop corrections in the (N)MSSM are sizable at the level of -10%, i.e. far larger than any anticipated accuracy of the experimental coupling determination. On the other hand, the deviation between the NMSSM and MSSM is tiny, below the level of 0.1%, once the Higgs-boson mass is fixed to its experimental value of about 125 GeV.

5 Conclusions

We evaluated the light neutral (N)MSSM Higgs boson production mode at e^+e^- colliders with a two-particle final state, i.e. $e^+e^- \to h_1 Z$, allowing for complex parameters. A precise prediction of this Higgs-boson production cross section is crucial for the high-precision determination of the Higgs-boson couplings expected at future e^+e^- colliders. In order to yield a sufficient accuracy, at least the one-loop corrections to the various Higgs boson production modes (and possibly in a further step also non-factorization effects) have to be considered.

Our evaluation of the Higgs-boson production process in association with a Z boson is based on a full one-loop calculation, also including hard, soft and collinear QED radiation.

[11] Technically there is a division by $\cos(\varphi_\kappa + 3\varphi_{\mu_{\text{eff}}} - 3\varphi_\lambda)$ in the code of NMSSMCALC (we note that our notation of the phases is slightly different from NMSSMCALC). While varying φ_λ we keep $\varphi_\kappa = \varphi_{\mu_{\text{eff}}} = 0$. Therefore this cosine becomes zero at $\varphi_\lambda = 30°, 90°, \ldots, 330°$ finally leading to $m^2_{h_1} < 0$.

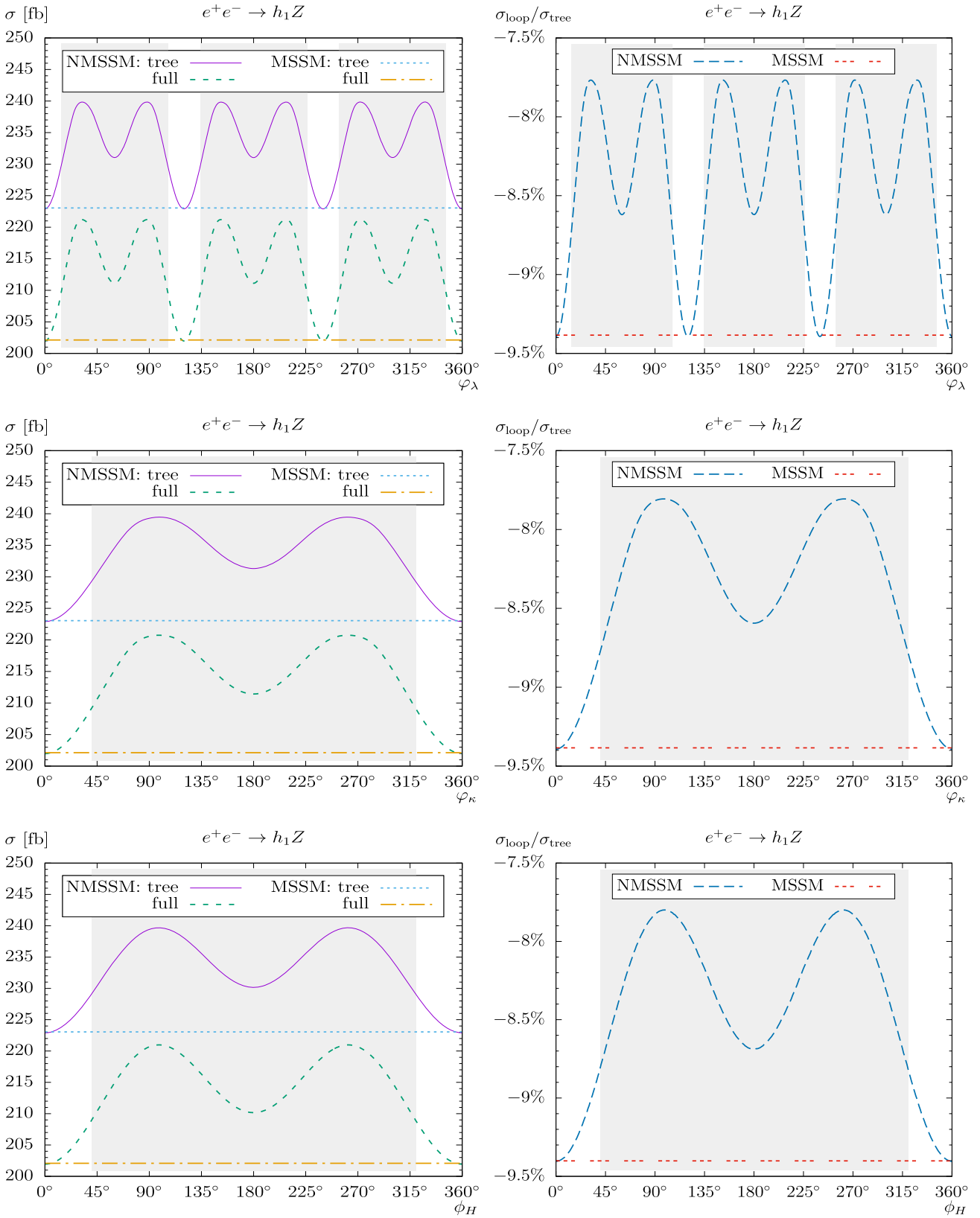

Fig. 8 $\sigma(e^+e^- \to h_1 Z)$. Tree-level and full one-loop corrected cross sections in the (N)MSSM are shown with parameters chosen according to Table 1. The upper plots show the cross sections with the phase φ_λ varied (left) and the corresponding $\sigma_{\text{loop}}/\sigma_{\text{tree}}$ in percent (right); the middle plots show the cross sections with the phase φ_κ varied (left) and the corresponding $\sigma_{\text{loop}}/\sigma_{\text{tree}}$ in percent (right); the lower plots show the phase ϕ_H varied (left) and the corresponding $\sigma_{\text{loop}}/\sigma_{\text{tree}}$ in percent (right). The light-gray area is excluded by $m_{h_1} < 123.5$ GeV

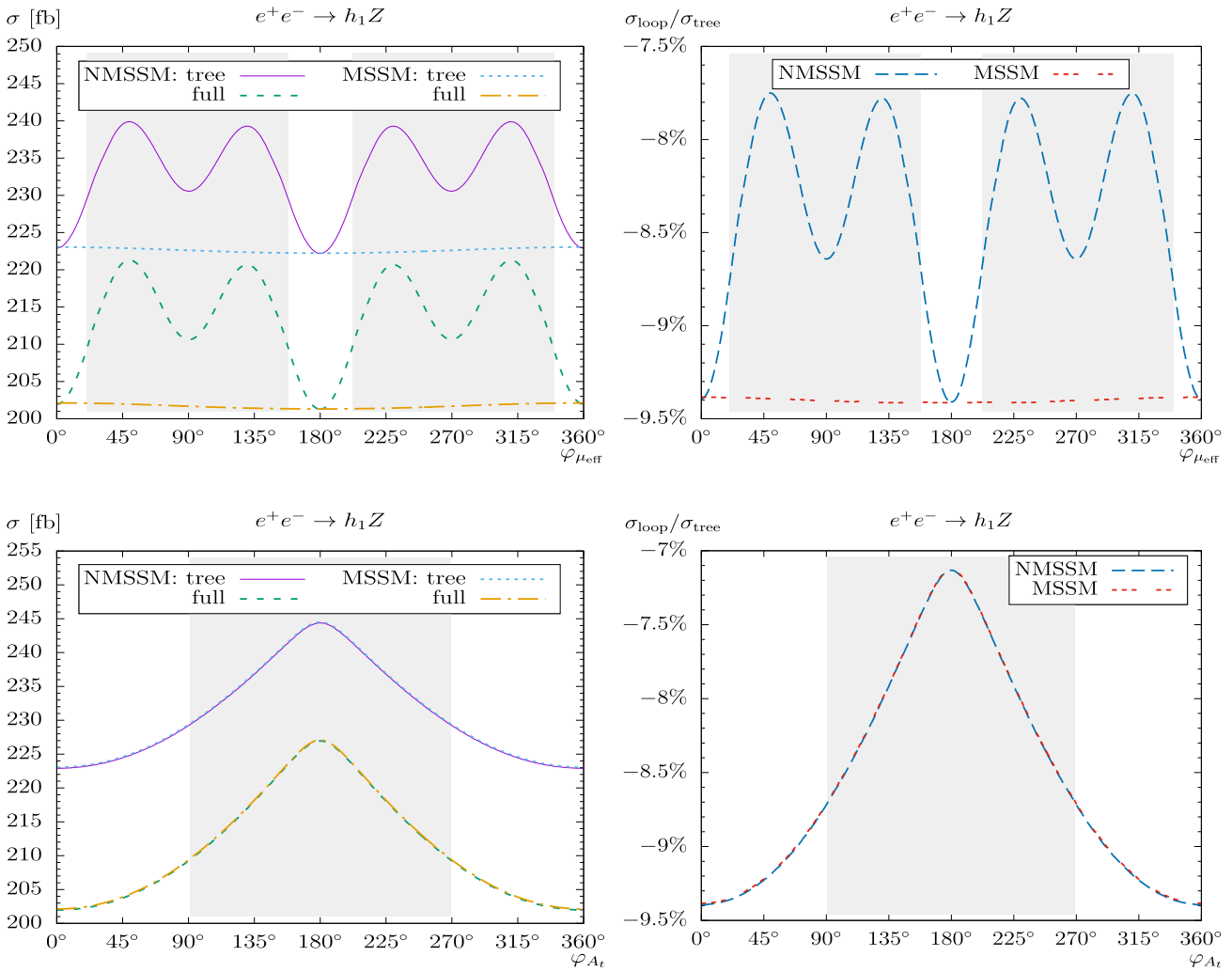

Fig. 9 $\sigma(e^+e^- \to h_1 Z)$. Tree-level and full one-loop corrected cross sections in the (N)MSSM are shown with parameters chosen according to Table 1. The upper plots show the cross sections with the phase $\varphi_{\mu_{\text{eff}}}$ varied (left) and the corresponding $\sigma_{\text{loop}}/\sigma_{\text{tree}}$ in percent (right); the lower plots show the phase φ_{A_t} varied (left) and the corresponding $\sigma_{\text{loop}}/\sigma_{\text{tree}}$ in percent (right). The light-gray area is excluded by $m_{h_1} \approx M_h < 123.5$ GeV

The renormalization is chosen to be identical as for the various Higgs boson decay calculations; see, e.g., Refs. [46,47]. This allows a consistent evaluation of the cross section times branching ratio, as it is required for a precise determination of the Higgs-boson couplings.

We first very briefly reviewed the relevant sectors including some details of the one-loop renormalization procedure of the cNMSSM, which are relevant for our calculation. In most cases we follow [28,88]. We have discussed the calculation of the one-loop diagrams, the treatment of UV, IR, and collinear divergences that are canceled by the inclusion of (hard, soft, and collinear) QED radiation. We have checked our result against the literature, and found qualitative agreement where possible.

For the numerical analysis we have chosen a parameter set that yields a light NMSSM Higgs-boson mass of $m_{h_1} \approx 125$ GeV for a large variation of the relevant parameters. Concerning the MSSM, the results have been obtained in the MSSM-limit of the NMSSM ($\lambda \to 0, \kappa \to 0$ with λ/κ fixed, and $\phi_H \to 0$), the light Higgs-boson mass is accordingly found at the value of $M_h \approx 125$ GeV for the relevant parts of the parameter space (in our benchmark scenario (see Tab. 1) we always have $h_1 \sim h$). In our plots the areas with $m_{h_1} < 123.5$ GeV (or $M_h < 123.5$ GeV) are indicated (and not taken into account in the discussion). In the analysis we investigated the variation of the production cross sections with the center-of-mass energy $\sqrt{s}$, the genuine NMSSM parameters λ, κ, A_κ, as well as with $M_{H^\pm}$, μ_{eff}, $M_{\tilde{Q}_3}$, $M_{\tilde{U}_3}$ and A_t. We have also analyzed the effects of the phases φ_λ,

φ_κ, $\varphi_{\mu_{\rm eff}}$ and φ_{A_t}. For all these analysis (except the variation with $\sqrt{s}$) we have set the center-of-mass energy to the first stage value of most of the possible future e^+e^- colliders, $\sqrt{s} = 250$ GeV.

The loop corrections in the (N)MSSM are found to be sizable, at the level of -10%. i.e. far larger than any anticipated accuracy of the experimental coupling determination. On the other hand, the observed variations (mostly in the NMSSM) are very small and (nearly) purely kinematic, originating from the small variation allowed in m_{h_1} due to the theoretical uncertainties, see [30]. However, since the value of the Higgs-boson mass is determined experimentally to a high accuracy, these kinematic effects must be considered numerical artefacts. The only genuine loop effects of the NMSSM w.r.t. the MSSM were observed in the dependence on $M_{\tilde{Q}_3}$, $M_{\tilde{U}_3}$ and A_t, but well below the %-level. This also holds for the variation with the phases included in our analysis.

The numerical results we have shown are, of course, dependent on the choice of the SUSY parameters. Nevertheless, they give an idea of the relevance of the full one-loop corrections. Following our analysis it is evident that the full one-loop corrections are mandatory for a precise prediction of the light c(N)MSSM Higgs boson production in association with a Z boson. The full one-loop corrections must be taken into account in any precise determination of (SUSY) parameters from the production of c(N)MSSM Higgs bosons at future e^+e^- colliders. There are plans to implement the evaluation of the Higgs boson production into the public code `FeynHiggs`.

Acknowledgements We thank T. Hahn for his help implementing `NMSSMCALC` into `FormCalc`. The work of S.H. has received financial support from the grant PID2019-110058GB-C21 funded by MCIN/AEI/10.13039/501100011033 and by "ERDF A way of making Europe", and in part by the grant IFT Centro de Excelencia Severo Ochoa CEX2020-001007-S funded by MCIN/AEI/10.13039/501100011033. S.H. also acknowledges support from Grant PID2022-142545NB-C21 funded by MCIN/AEI/10.13039/501100011033/FEDER, UE.

Data Availability Statement This manuscript has no associated data. [Authors' comment: Data sharing not applicable to this article as no datasets were generated or analysed during the current study.]

Code Availability Statement Code/software will be made available on reasonable request. [Authors' comment: The code/software generated during and/or analysed during the current study is available from the corresponding author on reasonable request.]

Funded by SCOAP^3.

Appendix

We briefly demonstrate that Eq. 22 corresponds to Eq. 21 in the "limit $i \to 1$":

$$
\begin{aligned}
&\lim_{\substack{m\to\bar{m}\\ i\to 1}} \frac{m_{h_1}^2 - \bar{m}_{h_1}^2 + m_{h_1}^2 - \bar{m}_{h_i}^2}{m_{h_1}^2 - m_{h_i}^2} \\
&= \lim_{\substack{\epsilon_i\to\epsilon_1\to 0\\ i\to 1}} \frac{(\bar{m}_{h_1}+\epsilon_1)^2 - \bar{m}_{h_1}^2 + (\bar{m}_{h_1}+\epsilon_1)^2 - \bar{m}_{h_i}^2}{(\bar{m}_{h_1}+\epsilon_1)^2 - (\bar{m}_{h_i}+\epsilon_i)^2} \\
&= \lim_{\substack{\epsilon_i\to\epsilon_1\to 0\\ i\to 1}} \frac{(\bar{m}_{h_1}^2 + 2\bar{m}_{h_1}\epsilon_1 + \epsilon_1^2) - \bar{m}_{h_1}^2 + (\bar{m}_{h_1}^2 + 2\bar{m}_{h_1}\epsilon_1 + \epsilon_1^2) - \bar{m}_{h_i}^2}{(\bar{m}_{h_1}^2 + 2\bar{m}_{h_1}\epsilon_1 + \epsilon_1^2) - (\bar{m}_{h_i}^2 + 2\bar{m}_{h_i}\epsilon_i + \epsilon_i^2)} \\
&= \lim_{\substack{\epsilon_i\to\epsilon_1\to 0\\ i\to 1}} \frac{(2\bar{m}_{h_1}\epsilon_1 + \epsilon_1^2) + (\bar{m}_{h_1}^2 + 2\bar{m}_{h_1}\epsilon_1 + \epsilon_1^2) - \bar{m}_{h_i}^2}{(\bar{m}_{h_1}^2 + 2\bar{m}_{h_1}\epsilon_1 + \epsilon_1^2) - (\bar{m}_{h_i}^2 + 2\bar{m}_{h_i}\epsilon_i + \epsilon_i^2)} \\
&= \lim_{\substack{\epsilon_i\to\epsilon_1\to 0\\ i\to 1}} \frac{2\bar{m}_{h_1}\epsilon_1 + \epsilon_1^2 + \bar{m}_{h_1}^2 + 2\bar{m}_{h_1}\epsilon_1 + \epsilon_1^2 - \bar{m}_{h_i}^2}{\bar{m}_{h_1}^2 + 2\bar{m}_{h_1}\epsilon_1 + \epsilon_1^2 - \bar{m}_{h_i}^2 - 2\bar{m}_{h_i}\epsilon_i - \epsilon_i^2} \\
&= \lim_{\substack{\epsilon_i\to\epsilon_1\to 0\\ i\to 1}} \frac{\bar{m}_{h_1}^2 - \bar{m}_{h_i}^2 + 4\bar{m}_{h_1}\epsilon_1 + 2\epsilon_1^2}{\bar{m}_{h_1}^2 - \bar{m}_{h_i}^2 + 2\bar{m}_{h_1}\epsilon_1 + \epsilon_1^2 - 2\bar{m}_{h_i}\epsilon_i - \epsilon_i^2} \\
&= \lim_{\substack{\epsilon_i\to\epsilon_1\to 0\\ i\to 1}} \frac{\bar{m}_{h_1}^2 - \bar{m}_{h_i}^2 + 4\bar{m}_{h_1}\epsilon_1 + 2\epsilon_1^2}{\bar{m}_{h_1}^2 - \bar{m}_{h_i}^2 + 2\bar{m}_{h_1}\epsilon_1 + \epsilon_1^2 - 2\bar{m}_{h_i}\epsilon_i - \epsilon_i^2} \\
&= \lim_{i\to 1} \frac{\bar{m}_{h_1}^2 - \bar{m}_{h_i}^2}{\bar{m}_{h_1}^2 - \bar{m}_{h_i}^2} = 1.
\end{aligned}
$$

References

1. G. Aad et al. [ATLAS Collaboration], Phys. Lett. B **716**, 1 (2012). arXiv:1207.7214 [hep-ex]
2. S. Chatrchyan et al. [CMS Collaboration], Phys. Lett. B **716**, 30 (2012). arXiv:1207.7235 [hep-ex]
3. G. Aad et al. [ATLAS], Nature **607**(7917), 52–59 (2022). [erratum: Nature **612**(7941), E24 (2022)]. arXiv:2207.00092 [hep-ex]
4. A. Tumasyan et al. [CMS], Nature **607**(7917), 60–68 (2022). [erratum: Nature **623**(7985), E4 (2023)]. arXiv:2207.00043 [hep-ex]
5. P. Fayet, S. Ferrara, Phys. Rep. **32**, 249–334 (1977)
6. P. Fayet, Phys. Lett. B **69**, 489 (1977)
7. H. Nilles, Phys. Rep. **110**, 1 (1984)
8. R. Barbieri, Riv. Nuovo Cim. **11**, 1 (1988)
9. H. Haber, G. Kane, Phys. Rep. **117**, 75 (1985)
10. J. Gunion, H. Haber, Nucl. Phys. B **272**, 1 (1986)
11. M. Maniatis, Int. J. Mod. Phys. A **25**, 3505 (2010). arXiv:0906.0777 [hep-ph]
12. U. Ellwanger, C. Hugonie, A.M. Teixeira, Phys. Rep. **496**, 1 (2010). arXiv:0910.1785 [hep-ph]
13. P. Fayet, Nucl. Phys. B **90**, 104–124 (1975)
14. J.E. Kim, H.P. Nilles, Phys. Lett. B **138**, 150 (1984)
15. J.R. Ellis, K. Enqvist, D.V. Nanopoulos, K.A. Olive, M. Quiros, F. Zwirner, Phys. Lett. B **176**, 403–408 (1986)
16. B. Rai, G. Senjanovic, Phys. Rev. D **49**, 2729–2733 (1994). arXiv:hep-ph/9301240

17. S. Abel, S. Sarkar, P. White, Nucl. Phys. B **454**, 663–684 (1995). arXiv:hep-ph/9506359
18. J. McDonald, Nucl. Phys. B **530**, 325–345 (1998). arXiv:hep-ph/9709512
19. C. Panagiotakopoulos, K. Tamvakis, Phys. Lett. B **446**, 224–227 (1999). arXiv:hep-ph/9809475
20. K. Hamaguchi, K. Nakayama, N. Yokozaki, Phys. Lett. B **708**, 100–106 (2012). arXiv:1107.4760 [hep-ph]
21. H. Hattori, T. Kobayashi, N. Omoto, O. Seto, Phys. Rev. D **92**(10), 103518 (2015). arXiv:1510.03595 [hep-ph]
22. A. Mazumdar, K. Saikawa, M. Yamaguchi, J. Yokoyama, Phys. Rev. D **93**(2), 025002 (2016). arXiv:1511.01905 [hep-ph]
23. A. Pilaftsis, Phys. Rev. D **58**, 096010 (1998). arXiv:hep-ph/9803297
24. A. Pilaftsis, Phys. Lett. B **435**, 88 (1998). arXiv:hep-ph/9805373
25. D. Demir, Phys. Rev. D **60**, 055006 (1999). arXiv:hep-ph/9901389
26. A. Pilaftsis, C. Wagner, Nucl. Phys. B **553**, 3 (1999). arXiv:hep-ph/9902371
27. S. Heinemeyer, Eur. Phys. J. C **22**, 521 (2001). arXiv:hep-ph/0108059
28. F. Domingo, P. Drechsel, S. Paßehr, Eur. Phys. J. C **77**(8), 562 (2017). arXiv:1706.00437 [hep-ph]
29. S. Heinemeyer, O. Stål, G. Weiglein, Phys. Lett. B **710**, 201 (2012). arXiv:1112.3026 [hep-ph]
30. P. Slavich, S. Heinemeyer (eds.), E. Bagnaschi et al., Eur. Phys. J. C **81**(5), 450 (2021). arXiv:2012.15629 [hep-ph]
31. A. Abada et al. [FCC], Eur. Phys. J. ST **228**(2), 261–623 (2019)
32. See: https://home.cern/science/accelerators/future-circular-collider
33. J.B. Guimarães da Costa et al. [CEPC Study Group], arXiv:1811.10545 [hep-ex]
34. X. Ai et al. arXiv:2505.24810 [hep-ex]
35. See: http://cepc.ihep.ac.cn
36. See: https://www.linearcollider.org
37. G. Moortgat-Pick et al., Eur. Phys. J. C **75**(8), 371 (2015). arXiv:1504.01726 [hep-ph]
38. D. Attié et al. [Linear Collider Vision], arXiv:2503.19983 [hep-ex]
39. A. Subba et al. [Linear Collider Facility at CERN], arXiv:2503.24049 [hep-ex]
40. See: https://clic.cern
41. S. Heinemeyer, C. Schappacher, Eur. Phys. J. C **76**(4), 220 (2016). arXiv:1511.06002 [hep-ph]
42. F. Arco, S. Heinemeyer, C. Schappacher, arXiv:2002.06905 [hep-ph]
43. S. Kanemura, K. Mawatari, K. Sakurai, Phys. Rev. D **99**(3), 035023 (2019). arXiv:1808.10268 [hep-ph]
44. J. de Blas et al., JHEP **01**, 139 (2020). arXiv:1905.03764 [hep-ph]
45. K. Williams, H. Rzehak, G. Weiglein, Eur. Phys. J. C **71**, 1669 (2011). arXiv:1103.1335 [hep-ph]
46. S. Heinemeyer, C. Schappacher, Eur. Phys. J. C **75**(5), 198 (2015). arXiv:1410.2787 [hep-ph]
47. S. Heinemeyer, C. Schappacher, Eur. Phys. J. C **75**(5), 230 (2015). arXiv:1503.02996 [hep-ph]
48. S. Heinemeyer, W. Hollik, G. Weiglein, Eur. Phys. J. C **16**, 139 (2000). arXiv:hep-ph/0003022
49. R. Hempfling, Phys. Rev. D **49**, 6168 (1994)
50. L. Hall, R. Rattazzi, U. Sarid, Phys. Rev. D **50**, 7048 (1994). arXiv:hep-ph/9306309
51. M. Carena, M. Olechowski, S. Pokorski, C. Wagner, Nucl. Phys. B **426**, 269 (1994). arXiv:hep-ph/9402253
52. M. Carena, D. Garcia, U. Nierste, C. Wagner, Nucl. Phys. B **577**, 577 (2000). arXiv:hep-ph/9912516
53. D. Noth, M. Spira, Phys. Rev. Lett. **101**, 181801 (2008). arXiv:0808.0087 [hep-ph]
54. D. Noth, M. Spira, JHEP **1106**, 084 (2011). arXiv:1001.1935 [hep-ph]
55. W. Hollik, J. Zhang, Phys. Rev. D **84**, 055022 (2011). arXiv:1109.4781 [hep-ph]
56. A. Bredenstein, A. Denner, S. Dittmaier, M. Weber, Phys. Rev. D **74**, 013004 (2006). arXiv:hep-ph/0604011
57. A. Bredenstein, A. Denner, S. Dittmaier, M. Weber, JHEP **0702**, 080 (2007). arXiv:hep-ph/0611234
58. A. Bredenstein, A. Denner, S. Dittmaier, A. Mück, M. Weber, see: https://omnibus.uni-freiburg.de/~sd565/programs/prophecy4f/prophecy4f.html
59. M. Frank, T. Hahn, S. Heinemeyer, W. Hollik, H. Rzehak, G. Weiglein, JHEP **0702**, 047 (2007). arXiv:hep-ph/0611326
60. S. Heinemeyer, W. Hollik, G. Weiglein, Comput. Phys. Commun. **124**, 76 (2000). arXiv:hep-ph/9812320
61. T. Hahn, S. Heinemeyer, W. Hollik, H. Rzehak, G. Weiglein, Comput. Phys. Commun. **180**, 1426 (2009)
62. H. Bahl, T. Hahn, S. Heinemeyer, W. Hollik, S. Paßehr, H. Rzehak, G. Weiglein, Comput. Phys. Commun. **249**, 107099 (2020). arXiv:1811.09073 [hep-ph]. see: http://www.feynhiggs.de
63. S. Heinemeyer, W. Hollik, G. Weiglein, Eur. Phys. J. C **9**, 343 (1999). arXiv:hep-ph/9812472
64. G. Degrassi, S. Heinemeyer, W. Hollik, P. Slavich, G. Weiglein, Eur. Phys. J. C **28**, 133 (2003). arXiv:hep-ph/0212020
65. T. Hahn, S. Heinemeyer, W. Hollik, H. Rzehak, G. Weiglein, Phys. Rev. Lett. **112**, 141801 (2014). arXiv:1312.4937 [hep-ph]
66. H. Bahl, W. Hollik, Eur. Phys. J. C **76**(9), 499 (2016). arXiv:1608.01880 [hep-ph]
67. H. Bahl, S. Heinemeyer, W. Hollik, G. Weiglein, Eur. Phys. J. C **78**(1), 57 (2018). arXiv:1706.00346 [hep-ph]
68. A. Djouadi, J. Kalinowsli, M. Spira, Comput. Phys. Commun. **108**, 56 (1998). arXiv:hep-ph/9704448
69. M. Spira, Fortschr. Phys. **46**, 203 (1998). arXiv:hep-ph/9705337
70. A. Djouadi et al. [HDECAY], Comput. Phys. Commun. **238**, 214–231 (2019). arXiv:1801.09506 [hep-ph]
71. S. Heinemeyer et al. [LHC Higgs Cross Section Working Group], arXiv:1307.1347 [hep-ph]
72. F. Domingo, S. Heinemeyer, S. Paßehr, G. Weiglein, Eur. Phys. J. C **78**(11), 942 (2018). arXiv:1807.06322 [hep-ph]
73. F. Domingo, S. Paßehr, Eur. Phys. J. C **79**(11), 905 (2019). arXiv:1907.05468 [hep-ph]
74. J. Baglio, T.N. Dao, M. Mühlleitner, Eur. Phys. J. C **80**(10), 960 (2020). arXiv:1907.12060 [hep-ph]
75. T.N. Dao, L. Fritz, M. Krause, M. Mühlleitner, S. Patel, Eur. Phys. J. C **80**(3), 292 (2020). arXiv:1911.07197 [hep-ph]
76. F. Domingo, S. Paßehr, Eur. Phys. J. C **80**(12), 1124 (2020). arXiv:2007.11010 [hep-ph]
77. T.N. Dao, M. Muhlleitner, S. Patel, K. Sakurai, Eur. Phys. J. C **81**(4), 340 (2021). arXiv:2012.14889 [hep-ph]
78. T.N. Dao, M. Muhlleitner, S. Patel, K. Sakurai, arXiv:2105.08454 [hep-ph]
79. F. Domingo, S. Paßehr, Eur. Phys. J. C **82**(10), 962 (2022). arXiv:2207.05776 [hep-ph]
80. S. Heinemeyer, C. Schappacher, arXiv:1602.08041 [hep-ph]
81. J. Baglio, R. Gröber, M. Mühlleitner, D.T. Nhung, H. Rzehak, M. Spira, J. Streicher, K. Walz, Comput. Phys. Commun. **185**, 12 (2014). arXiv:1312.4788 [hep-ph]]
82. K. Ender, T. Graf, M. Mühlleitner, H. Rzehak, Phys. Rev. D **85**, 075024 (2012). arXiv:1111.4952 [hep-ph]
83. T. Graf, R. Gröber, M. Mühlleitner, H. Rzehak, K. Walz, JHEP **10**, 122 (2012). arXiv:1206.6806 [hep-ph]
84. M. Mühlleitner, D.T. Nhung, H. Rzehak, K. Walz, JHEP **05**, 128 (2015). arXiv:1412.0918 [hep-ph]
85. T.N. Dao, R. Gröber, M. Krause, M. Mühlleitner, H. Rzehak, JHEP **08**, 114 (2019). arXiv:1903.11358 [hep-ph]. Program and

explanations are available via: https://www.itp.kit.edu/~maggie/NMSSMCALC/
86. S.W. Ham, S.H. Kim, S.k. Oh, D. Son, Phys. Rev. D **76**, 115013 (2007). arXiv:0708.2755 [hep-ph]
87. J. Cao, C. Han, J. Ren, L. Wu, J.M. Yang, Y. Zhang, Chin. Phys. C **40**(11), 113104 (2016). arXiv:1410.1018 [hep-ph]
88. T. Fritzsche, T. Hahn, S. Heinemeyer, F. von der Pahlen, H. Rzehak, C. Schappacher, Comput. Phys. Commun. **185**, 1529 (2014). arXiv:1309.1692 [hep-ph]
89. S. Heinemeyer, H. Rzehak, C. Schappacher, Phys. Rev. D **82**, 075010 (2010). arXiv:1007.0689 [hep-ph]
90. S. Heinemeyer, H. Rzehak, C. Schappacher, PoSCHARGED **2010**, 039 (2010). arXiv:1012.4572 [hep-ph]
91. T. Fritzsche, S. Heinemeyer, H. Rzehak, C. Schappacher, Phys. Rev. D **86**, 035014 (2012). arXiv:1111.7289 [hep-ph]
92. S. Heinemeyer, C. Schappacher, Eur. Phys. J. C **72**, 1905 (2012). arXiv:1112.2830 [hep-ph]
93. S. Heinemeyer, C. Schappacher, Eur. Phys. J. C **72**, 2136 (2012). arXiv:1204.4001 [hep-ph]
94. S. Heinemeyer, F. von der Pahlen, C. Schappacher, Eur. Phys. J. C **72**, 1892 (2012). arXiv:1112.0760 [hep-ph]
95. S. Heinemeyer, F. von der Pahlen, C. Schappacher, arXiv:1202.0488 [hep-ph]
96. A. Bharucha, S. Heinemeyer, F. von der Pahlen, C. Schappacher, Phys. Rev. D **86**, 075023 (2012). arXiv:1208.4106 [hep-ph]
97. A. Bharucha, S. Heinemeyer, F. von der Pahlen, Eur. Phys. J. C **73**, 2629 (2013). arXiv:1307.4237 [hep-ph]
98. J. Küblbeck, M. Böhm, A. Denner, Comput. Phys. Commun. **60**, 165 (1990)
99. T. Hahn, Comput. Phys. Commun. **140**, 418 (2001). arXiv:hep-ph/0012260
100. T. Hahn, C. Schappacher, Comput. Phys. Commun. **143**, 54 (2002). arXiv:hep-ph/0105349. Program, user's guide and model files are available via: https://www.feynarts.de
101. T. Hahn, M. Pérez-Victoria, Comput. Phys. Commun. **118**, 153 (1999). arXiv:hep-ph/9807565. Program and user's guide are available via: https://www.feynarts.de/formcalc/
102. F. Domingo, S. Paßehr, Eur. Phys. J. C **81**(7), 661 (2021). arXiv:2105.01139 [hep-ph]
103. A. Denner, S. Dittmaier, M. Roth, D. Wackeroth, Nucl. Phys. B **560**, 33 (1999). arXiv:hep-ph/9904472.
104. M. Nowakowski, A. Pilaftsis, Z., Phys. C **60**, 121–126 (1993). arXiv:hep-ph/9305321
105. F. del Aguila, A. Culatti, R. Muñoz-Tapia, M. Pérez-Victoria, Nucl. Phys. B **537**, 561 (1999). arXiv:hep-ph/9806451
106. W. Siegel, Phys. Lett. B **84**, 193 (1979)
107. D. Capper, D. Jones, P. van Nieuwenhuizen, Nucl. Phys. B **167**, 479 (1980)
108. D. Stöckinger, JHEP **0503**, 076 (2005). arXiv:hep-ph/0503129
109. W. Hollik, D. Stöckinger, Phys. Lett. B **634**, 63 (2006). arXiv:hep-ph/0509298
110. A. Denner, Fortsch. Phys. **41**, 307 (1993). arXiv:0709.1075 [hep-ph]
111. K. Fabricius, I. Schmitt, G. Kramer, G. Schierholz, Zeit. Phys. C **11**, 315 (1981)
112. G. Kramer, B. Lampe, Fortschr. Phys. **37**, 161 (1989)
113. H. Baer, J. Ohnemus, J. Owens, Phys. Rev. D **40**, 2844 (1989)
114. B. Harris, J. Owens, Phys. Rev. D **65**, 094032 (2002). arXiv:hep-ph/0102128
115. T. Hahn, Comput. Phys. Commun. **168**, 78 (2005). arXiv:hep-ph/0404043
116. T. Hahn arXiv:1408.6373 [physics.comp-ph]. The program is available via: https://www.feynarts.de/cuba/
117. R.L. Workman et al. (Particle Data Group), Prog. Theor. Exp. Phys. **2022**, 083C01 (2022)
118. J. Frère, D. Jones, S. Raby, Nucl. Phys. B **222**, 11 (1983)
119. M. Claudson, L. Hall, I. Hinchliffe, Nucl. Phys. B **228**, 501 (1983)
120. C. Kounnas, A. Lahanas, D. Nanopoulos, M. Quiros, Nucl. Phys. B **236**, 438 (1984)
121. J. Gunion, H. Haber, M. Sher, Nucl. Phys. B **306**, 1 (1988)
122. J. Casas, A. Lleyda, C. Muñoz, Nucl. Phys. B **471**, 3 (1996). arXiv:hep-ph/9507294
123. P. Langacker, N. Polonsky, Phys. Rev. D **50**, 2199 (1994). arXiv:hep-ph/9403306
124. A. Strumia, Nucl. Phys. B **482**, 24 (1996). arXiv:hep-ph/9604417
125. S. Dimopoulos, S. Thomas, Nucl. Phys. B **465**, 23 (1996). arXiv:hep-ph/9510220
126. M. Dugan, B. Grinstein, L. Hall, Nucl. Phys. B **255**, 413 (1985)